RESEARCH ARTICLE

Open Access

Personalised modelling of clinical heterogeneity between medium-chain acyl-CoA dehydrogenase patients

Christoff Odendaal[1†], Emmalie A. Jager[1,2†], Anne-Claire M. F. Martines[1], Marcel A. Vieira-Lara[1],
Nicolette C. A. Huijkman[1], Ligia A. Kiyuna[1], Albert Gerding[1,3], Justina C. Wolters[1], Rebecca Heiner-Fokkema[3],
Karen van Eunen[1], Terry G. J. Derks[2*] and Barbara M. Bakker[1*]

Abstract

Background Monogenetic inborn errors of metabolism cause a wide phenotypic heterogeneity that may even differ between family members carrying the same genetic variant. Computational modelling of metabolic networks may identify putative sources of this inter-patient heterogeneity. Here, we mainly focus on medium-chain acyl-CoA dehydrogenase deficiency (MCADD), the most common inborn error of the mitochondrial fatty acid oxidation (mFAO). It is an enigma why some MCADD patients—if untreated—are at risk to develop severe metabolic decompensations, whereas others remain asymptomatic throughout life. We hypothesised that an ability to maintain an increased free mitochondrial CoA (CoASH) and pathway flux might distinguish asymptomatic from symptomatic patients.

Results We built and experimentally validated, for the first time, a kinetic model of the human liver mFAO. Metabolites were partitioned according to their water solubility between the bulk aqueous matrix and the inner membrane. Enzymes are also either membrane-bound or in the matrix. This metabolite partitioning is a novel model attribute and improved predictions. MCADD substantially reduced pathway flux and CoASH, the latter due to the sequestration of CoA as medium-chain acyl-CoA esters. Analysis of urine from MCADD patients obtained during a metabolic decompensation showed an accumulation of medium- and short-chain acylcarnitines, just like the acyl-CoA pool in the MCADD model. The model suggested some rescues that increased flux and CoASH, notably increasing short-chain acyl-CoA dehydrogenase (SCAD) levels. Proteome analysis of MCADD patient-derived fibroblasts indeed revealed elevated levels of SCAD in a patient with a clinically asymptomatic state. This is a rescue for MCADD that has not been explored before. Personalised models based on these proteomics data confirmed an increased pathway flux and CoASH in the model of an asymptomatic patient compared to those of symptomatic MCADD patients.

Conclusions We present a detailed, validated kinetic model of mFAO in human liver, with solubility-dependent metabolite partitioning. Personalised modelling of individual patients provides a novel explanation for phenotypic

---

[†]Christoff Odendaal and Emmalie A. Jager contributed equally to this work.

*Correspondence:
Terry G. J. Derks
t.g.j.derks@umcg.nl
Barbara M. Bakker
b.m.bakker01@umcg.nl
Full list of author information is available at the end of the article

Odendaal *et al. BMC Biology*   (2023) 21:184

Page 2 of 22

heterogeneity among MCADD patients. Further development of personalised metabolic models is a promising direction to improve individualised risk assessment, management and monitoring for inborn errors of metabolism.

Keywords Medium-chain acyl-CoA dehydrogenase deficiency, Mitochondrial fatty acid oxidation, Personalised medicine, Metabolite partitioning, Kinetic modelling, Phenotypic heterogeneity, Inborn error of metabolism

Background

Inborn errors of metabolism (IEMs) are distinct monogenetic diseases that cause pronounced systemic aberrations. While individually rare, the over 1450 different IEMs together have serious consequences in terms of morbidity and mortality, especially in children [1]. A better understanding of metabolism and its regulation, therefore, has wide implications [2–4]. Computational kinetic modelling of biochemical pathways is a promising tool for understanding and predicting complex pathway behaviour. Ultimately, coupling computational models of individual pathways could form a comprehensive representation of human biochemistry in silico. This concept has variously been referred to as the 'Silicon Cell' or the 'Digital Twin' [5–8].

IEMs provide a logical starting point for studying metabolism due to the presence of well-defined causative genetic variations. People with IEMs show large phenotypic heterogeneity, even between individuals carrying the same genetic variant [9]. Medium-chain acyl-CoA dehydrogenase deficiency (MCADD; OMIM #201450), the most common mitochondrial fatty acid oxidation (mFAO) disorder (mFAOD), is an illustrative example [10].

The deficient enzyme in MCADD, medium-chain acyl-CoA dehydrogenase (MCAD; EC: 1.3.8.7; UniProtKB: P11310) is one of a triad of enzymes in human cells (together with short- and very-long-chain acyl-CoA dehydrogenases, SCAD and VLCAD, respectively) that catalyse the first step of the mFAO. These three enzymes have distinct but overlapping substrate specificity [11]. Mainly before the age of 5 years, MCADD poses the risk of life-threatening metabolic decompensations elicited by fasting and/or infections [12, 13]. These metabolic decompensations are characterised by hypoketotic hypoglycaemia, metabolic acidosis and hepatic dysfunction [10]. Symptomatic patients might present with lethargy, nausea and vomiting and rapidly progress to coma or seizures. Avoidance of fasting and the implementation of an emergency regimen during illness can prevent the development of these symptoms [14–17]. In nine out of ten clinically ascertained MCADD patients [9, 18], homozygosity for the common c.985G > A *ACADM* variant (< 1% residual MCAD activity) is found. But this variant is *also* seen in many clinically asymptomatic patients [9]. The introduction

of MCADD in newborn screening has substantially reduced morbidity and mortality [19, 20]. However, the newborn screening also identifies children with other *ACADM* variants, with higher residual MCAD activities, of which the clinical implications are incompletely understood. To improve individual patients' risk assessment, management and monitoring, a better understanding of what underlies the phenotypic heterogeneity is needed [21, 22].

*C*oA *s*equestration, *to*xicity or *r*edistribution (CASTOR) has previously been posited as a possible pathogenic mechanism in MCADD and a number of other IEMs with a similar phenotype [23, 24]. A computational kinetic model of mFAO in mouse liver suggested that a loss of MCAD activity can indeed make the mFAO vulnerable to free CoA (CoASH) depletion, as well as to a decline of mFAO flux [25–27].

CoASH depletion and flux decline could impair ketogenesis and cause hypoglycaemia. Under fasted conditions, ketogenesis supplements the body's energy needs by producing ketone bodies. To make ketone bodies, acetyl-CoA is used, of which around 85% comes from the mFAO [28]. The ketogenesis flux varies proportionally to the mFAO flux, increasing 1:1 when mFAO increases and vice versa [29–31]. Moreover, pharmacological inhibition of mFAO impairs gluconeogenesis [32]. This may be caused by the reduced availability of ATP for gluconeogenesis due to impaired mFAO flux [33, 34]. Alternatively, it may be due to a lack of gluconeogenic precursors, many of which are products or intermediates of the branched-chain amino acid degradation and tricarboxylic acid (TCA) cycle [34, 35]—both pathways that use CoASH as a substrate and would be impaired by CoASH depletion.

Here we developed a systems medicine approach to identify putative compensatory mechanisms in MCADD patients. We hypothesise that an ability to maintain sufficient mitochondrial CoASH and pathway flux might distinguish asymptomatic from symptomatic patients. Therefore, we constructed a computational, kinetic model of human liver mFAO—the first such model for human liver of which we are aware. Building on a previous model of mFAO in rat liver [26], we updated kinetic constants with human parameters, added two enzymes important to mitochondrial CoA metabolism. As an additional innovation, we made the

spatial partitioning of hydrophobic acyl-CoA esters between the mitochondrial matrix and the membrane-bound enzymes explicit. The model was validated against experimental data, including the profile of even-chain saturated acylcarnitines in MCADD patient crisis urine samples. To personalise the model, targeted proteomics data were collected from fibroblasts of MCADD patients and used to adjust model parameters. The personalised model of an asymptomatic MCADD individual showed proteomic adaptations that increased CoASH and pathway flux, mainly increased SCAD.

Results and discussion

Construction of a human mFAO model

We constructed a dynamic model of human mitochondrial fatty acid β-oxidation, including the carnitine shuttle and mitochondrial acyl-CoA thioesterase activity (Fig. 1). A detailed description of the model is available in Additional File 1: Text S1 [11, 25–27, 36–152].

As a starting point, we took an existing kinetic model of mFAO in rat liver, which has been validated quantitatively with detailed acylcarnitine time-course data [26]. The kinetic parameters, where possible, were replaced by human liver-derived values. Metabolite pools were modelled as being located either in the cytosol or in the mitochondrial matrix, with distinct volumes. Long-chain acyl-CoA dehydrogenase (LCAD), which is not expressed in human liver [87, 98, 109], was omitted. The model was extended with three enzymes important to mitochondrial CoA metabolism: carnitine acetyl-CoA transferase (CrAT [120]), a CoASH-sensitive acyl-CoA thioesterase (ACOTcs, based on the kinetics of
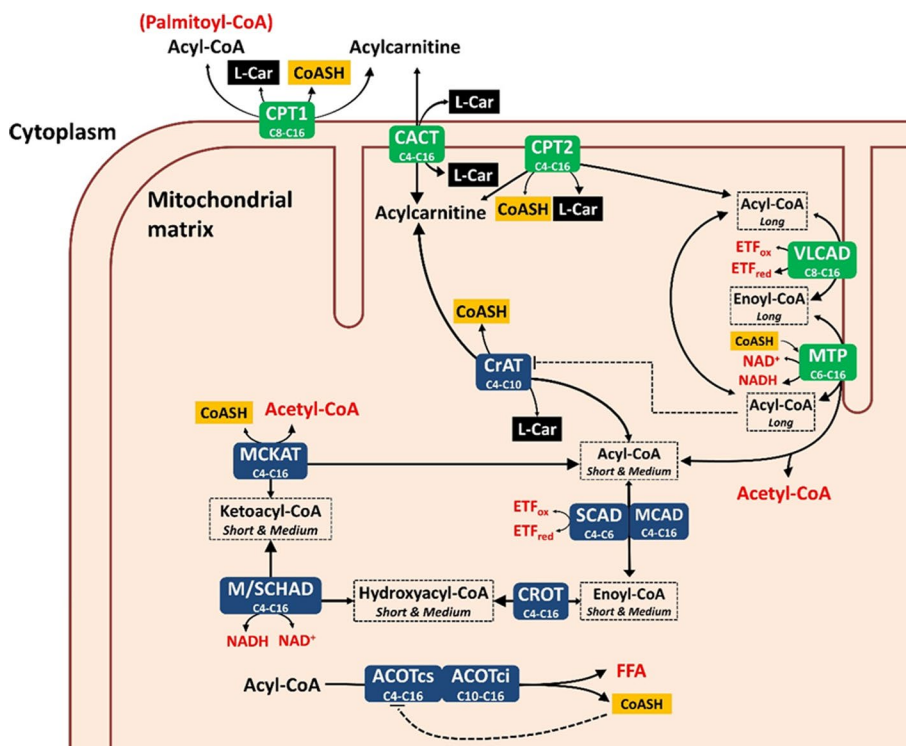

Fig. 1 Schematic overview of the human hepatic mitochondrial fatty acid oxidation model. Enzyme names are written in white with their chain length specificity as subscript (C16, for example, for a 16-carbon acyl group). The enzymes depicted in green are membrane-bound enzymes while the blue boxes indicate soluble enzymes. These enzymes interconvert metabolites (in black text). Subscripts identify the metabolites' chain lengths (*Long* or *Short & Medium*) and their primary localization according to their solubility. Metabolites in red are present at constant concentrations: ETF$_{ox}$ and ETF$_{red}$ refer to the oxidised and reduced form of the electron-transferring flavoprotein, and FFA indicates free fatty acids. Free coenzyme A (CoASH; yellow boxes) and L-carnitine (L-car; black boxes) are the non-acylated fraction of CoA and L-carnitine, of which the total pool forms a conserved moiety. The model includes the following enzymes: carnitine palmitoyltransferase 1a (CPT1; EC 2.3.1.21), carnitine/acylcarnitine translocase (CACT; PathwayCommons: O43772), carnitine palmitoyltransferase 2 (CPT2; EC 2.3.1.21), carnitine acetyltransferase (CrAT; EC 2.3.1.137), very-long-chain acyl-CoA dehydrogenase (VLCAD; EC 1.3.8.9), medium-chain acyl-CoA dehydrogenase (MCAD; EC 1.3.8.7), short-chain acyl-CoA dehydrogenase (SCAD; EC 1.3.8.1), crotonase (CROT; EC 4.2.1.17), medium- and short-chain hydroxyacyl-CoA dehydrogenase (M/SCHAD; EC 1.1.1.35), medium-chain ketoacyl-CoA thiolase (MCKAT; EC 2.3.1.16), mitochondrial trifunctional protein (MTP: EC 4.2.1.17, EC 1.1.1.211, EC 2.3.1.16), coenzyme A-insensitive acyl-CoA thioesterase (ACOTci; equivalent to ACOT2; EC 3.1.2.2), coenzyme A-sensitive acyl-CoA thioesterase (ACOTcs; equivalent to ACOT7 and ACOT13 combined; EC 3.1.2.2)

Odendaal *et al. BMC Biology*   (2023) 21:184

Page 4 of 22

ACOT7 and ACOT13) and a CoASH-insensitive one (ACOTci, representing ACOT2) [131].

Where human liver kinetic parameters were not available, the most suitable alternatives were chosen. Values from other human tissues were privileged. If measurements from human tissues were not available, parameters from other mammals were also considered. If tissue-specific isoforms exist (e.g. carnitine palmitoyltransferase 1, or CPT1 [153]), parameters from the liver of other mammals were preferred over human parameters from other tissues. We used equilibrium constants (K_{eq}) generated by the online tool eQuilibrator [66, 67]. Finally, all metabolites indicated in red in Fig. 1 were modelled as boundary metabolites with constant concentrations. This included acetyl-CoA, which was kept constant to allow the model to reach steady state. These constant boundary concentrations are model parameters, which can be varied in a realistic range, to assess their impact.

As a qualitative innovation, to reflect more accurately the physicochemical conditions inside the mitochondrion, we introduced partitioning of the mitochondrial metabolites between a water-soluble matrix pool and a hydrophobic mitochondrial inner-membrane pool. Longer acyl chains render metabolites less water-soluble, which causes a large fraction of the metabolite pool to localise to the membrane rather than dissolving in the aqueous matrix [55, 147, 152]. This would mean that membrane-embedded enzymes (green boxes in Fig. 1) would encounter a higher local concentration of these more hydrophobic intermediates, while soluble, matrix-localised enzymes (blue boxes in Fig. 1) would be exposed to a lower concentration of hydrophobic metabolites. Water-soluble metabolites, on the other hand, would diffuse more evenly throughout the mitochondrion, meaning that membrane-bound and soluble enzymes would be exposed to a similar, more dilute, concentration. It has been proposed that long-chain, hydrophobic acyl-CoAs 'surface crawl' along the mitochondrial inner membrane from active site to active site instead of diffusing into the bulk aqueous medium after each reaction [37, 38, 50, 133]. To mimic this phenomenon in the computational model, chain-length-specific 'relative partitioning factors' were introduced, which effectively split each mitochondrial metabolite pool into a fraction that reacts with the membrane-bound enzymes and one that reacts with matrix-localised enzymes. Enzymes were then also assigned a localisation—either membrane-bound or in the matrix. A more detailed discussion of the underlying assumptions and physical basis of metabolite partitioning is presented in the model description in Additional File 1: Text S1.

The final model contains the mitochondrial fatty acid oxidation reactions that pertain to even-chain, saturated acyl esters of 16 carbons or shorter [154]. All rate equations in the final model are reversible, except for those of ACOTci and ACOTcs, for which no reverse activity has been described [131]. Model simulations predict steady-state fluxes, metabolite concentrations, and dynamic rates. The model contains 49 variable metabolite concentrations, 75 reactions and 369 experimentally obtained parameters.

Model validation

Steady-state fluxes and reaction rates were then simulated and compared to three sets of experimental and MCADD patient data. Details of unit conversions and simulation conditions are given in full in Additional File 2: Text S2 [28, 29, 69, 78, 84, 92, 97, 101, 155–163].

First, oxygen consumption with palmitoyl-CoA as a substrate was measured in permeabilised control and MCAD-knockout (KO) HepG2 cells and compared to the fluxes predicted by the model (Fig. 2A). The knockouts were generated with CRISPR-Cas9 [164] and confirmed with genotyping (Additional File 3: Table S1), Western blot (Additional File 4: Fig. 1A) and proteomics (Additional File 4: Fig. 1B).

Since the reference model is based on human liver and these experiments were performed on HepG2s, the model was adapted based on literature-derived differences in protein concentration between healthy primary human hepatocytes and HepG2 cells [78, 159]. This was done by adjusting the V_{max} values in the model, which are linearly related to the corresponding enzyme concentrations. The effect of including metabolite partitioning and HepG2 proteomics in the model was assessed separately and in combination. The healthy control model predicted pathway flux within the range of the experimentally measured values after the inclusion of both metabolite partitioning factors and the adjustment of V_{max} values to HepG2 proteomics. Experimentally, the MCAD knockout reduced the mean O_2 consumption by 30%, which was best reproduced by simulation when both metabolite partitioning and HepG2 proteomics were included in the model (Fig. 2A). The correspondence between the model and the experiment is encouraging, particularly in the light of the fact that proteomics data were from an independent study.

Second, we predicted whole-body ketogenic flux from the model simulations. Although the model does not directly predict ketogenic flux, the rate of acetyl-CoA production dictates the maximum rate of ketone body synthesis from fatty acids [29–31]. Fletcher et al. [28] measured whole-body ketogenic flux using stable isotope-labelled substrates in healthy adults after 24 h of fasting ($n=17$). The ketogenic flux was predicted within the measured range by the human model, with
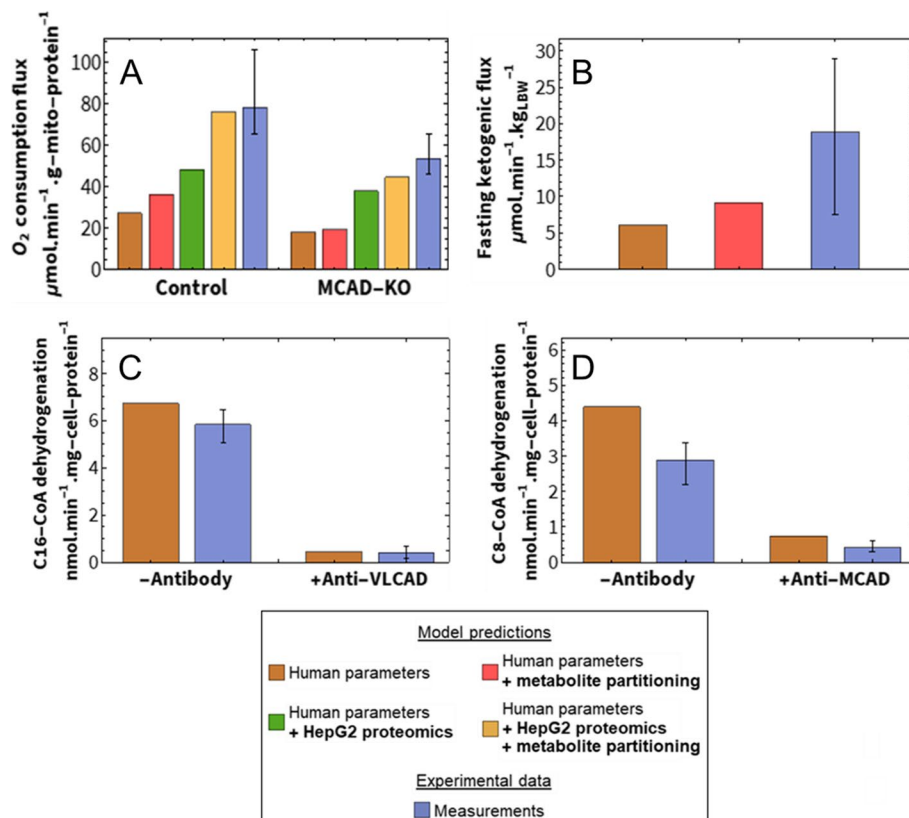
Fig. 2 Model validation. Model predictions compared to experimentally measured data (blue). All model adjustments and conversions are described in Additional File 2: Text S2. The bars represent the mean of the different data, while error bars indicate the range of the data (minimum and maximum). **A** Simulated NADH production flux, stoichiometrically converted to O_2 consumption, compared to the uncoupled oxygen consumption flux of permeabilised MCAD-KO and control HepG2 cells. In converting an NADH production flux to an oxygen consumption flux, the contribution of $FADH_2$ and reducing equivalents from the downstream TCA cycle were also considered (Additional File 2: Text S2). The experiment and simulation contained 25 μM of palmitoyl-CoA and 2 mM of L-carnitine (blue; $n = 4$ in both groups). **B** Simulated acetyl-CoA production flux, stoichiometrically converted to a ketogenic flux, compared to measured ketogenesis in 24 h-fasted, healthy human subjects ($n = 17$). **C, D** Comparison of simulated and measured palmitoyl-CoA (C16-CoA, **C**) and octanoyl-CoA (C8-CoA, **D**) dehydrogenation rates (acyl-CoA substrate at 30 μM) in crude lysate compared to cell lysates after immunoprecipitation of VLCAD or MCAD, respectively (blue; $n = 3$ or $n = 4$)

the prediction from the model including metabolite partitioning more closely approximating the mean of the measurements (Fig. 2B). That the predictions are at the lower end of the measured values might be partially explained by 'pseudoketogenesis': a methodological issue that leads to artificially high ketogenic flux measurements [165, 166]. No suitable quantification of this phenomenon was available, to our knowledge, so we could not correct for it in the model itself; however, it does explain why our model predictions fall at the lower end of the measured range.

Third, in vitro octanoyl- and palmitoyl-CoA dehydrogenation rates were predicted. Aoyama et al. [97] measured these rates in crude human liver lysate (− antibody in Fig. 2D) and in lysate with immunologically inactivated VLCAD or MCAD (+ anti-VLCAD and + anti-MCAD, respectively). We mimicked the immunological inactivation of VLCAD and MCAD

in the computational model by setting the maximum velocity (V_{max}) of the inactivated enzyme to zero. Since the assay was performed in tissue lysate, in the absence of membranes, metabolite partitioning was not considered. The palmitoyl-CoA dehydrogenation rate and the effect of VLCAD inactivation were predicted within 5% of the measured range (Fig. 2C). The octanoyl-CoA dehydrogenation rate for both the crude and the MCAD-inactivated lysates was overpredicted by about 30%; however, both the model prediction and the measured data showed an 85% reduction of this rate upon MCAD inactivation (Fig. 2D). The discrepancy between the measured and predicted rates of octanoyl-CoA dehydrogenation might be explained by natural variation in gene expression, which can be quite large among mitochondrial enzymes [167]. Considering this natural variation, the agreement that we did find was already good.

Taken together, Fig. 2 shows that experimental data across different scales, ranging from lysates to cells to whole-body data, are reliably predicted by the model. A realistic representation of metabolite partitioning between the mitochondrial matrix and the hydrophobic space close to the membrane substantially improved the correspondence between the model and the experiments.

Modelling a metabolic decompensation in MCADD patients

An important question was how accurately, and under which conditions, the model mimics the characteristics of MCADD patients experiencing metabolic decompensation. The model predicts acyl-CoA concentrations in the liver, but these are not accessible in patients. It is often assumed, however, that acylcarnitine patterns in blood or urine qualitatively reflect the acyl-CoA profile in the mitochondria [26, 45]. Therefore, acylcarnitine concentrations were quantified in urine from clinically asymptomatic and symptomatic patients, collected under *fed*, *fasted* or *metabolic decompensation* conditions. All patients were diagnosed before MCADD was included

in the neonatal screening and symptomatic patients had not undergone any treatment or observation prior to the crisis, making this a precious and unique dataset. Asymptomatic patients were identified during proband follow-up after their siblings had been admitted to hospital with hypoketotic hypoglycaemia. Under fed and overnight fasted conditions, symptomatic and asymptomatic MCADD patients showed similar urinary acylcarnitine concentrations (Table 1 and Additional File 5: Table S2), with a characteristically increased C8 compared to other metabolites [168]. In healthy controls, C8 is at comparable levels to other acylcarnitines [169]. Acylcarnitine accumulation also seemed unaffected by an overnight fast. During a metabolic decompensation, the total concentration of acylcarnitines increased and the C8/C10 ratio reached its highest levels. The increased acylcarnitines mainly comprised free carnitine, acetyl-, hexanoyl- and octanoylcarnitine (Table 1).

We then compared the patterns of measured urinary acylcarnitines to liver mitochondrial acyl-CoAs predicted by model simulation under stress. To mimic stress, the cytosolic palmitoyl-CoA concentration was set to

Table 1 Patient urine acylcarnitine profiles

Parameter in µmol/mmol creatinine	Asymptomatic. $n = 4$ Median (min.–max.)		Symptomatic. $n = 3$ Median (min.–max.)		
	Fed	**Fasted**	**Fed**	**Fasted**	**Decompensation**
Total acylcarnitine	3.19 (2.93–37.49)	2.72 (2.04–4.84)	5.83 (2.16–30.92)	1.87 (1.56–9.94)	141.78 (28.03–198.87)
C0	0.95 (0.60–17.44)	0.47 (0.34–1.39)	2.36 (1.05–5.74)	0.63 (0.42–0.92)	27.15 (2.27–77.20)
C2	0.24 (0.18–8.77)	0.14 (0.09–0.94)	0.76 (0.11–18.68)	0.09 (0.02–5.08)	75.60 (8.11–98.28)
C4	0.22 (0.12–0.39)	0.14 (0.06–0.20)	0.14 (0.02–0.30)	0.03 (0.02–0.12)	1.17 (0.60–2.46)
C6	0.065 (0.04–0.74)	0.06 (0.04–0.09)	0.08 (0.01–0.50)	0.02 (0.01–0.23)	3.84 (0.58–4.06)
C8	0.295 (0.20–6.72)	0.26 (0.20–0.74)	0.67 (0.01–3.22)	0.16 (0.13–0.93)	8.34 (7.12–24.35)
C10:1	0.11 (0.07–0.55)	0.07 (0.05–0.11)	0.11 (0.03–0.52)	0.06 (0.03–0.15)	0.93 (0.38–1.57)
C10	0.04 (0.02–0.10)	0.04 (0.03–0.05)	0.05 (0.01–0.11)	0.02 (0.02–0.15)	0.53 (0.42–0.97)
C12	0.015 (0.01–0.04)	0.02 (0.01–0.02)	0.02 (0.01–0.03)	0.01 (0.01–0.03)	0.12 (0.07–0.25)
C14	n.d (n.d.–0.01)	n.d (n.d.)	n.d (n.d.–0.01)	n.d (n.d.–0.01)	0.15 (0.15–0.28)
C16	n.d (n.d.)	n.d (n.d.)	n.d (n.d.)	n.d (n.d.)	0.03 (0.01–0.03)
C8/C2	1.14 (0.77–1.29)	1.76 (0.79–2.89)	0.17 (0.09–0.88)	1.78 (0.18–6.50)	0.32 (0.08–0.88)
C8/C10	8.83 (7.20–67.20)	7.67 (6.25–14.80)	13.40 (1.00–29.27)	6.50 (6.20–8.00)	19.86 (13.43–25.10)

n.d. not detectable, i.e. < 0.01 µmol/mmol creatinine

Odendaal *et al. BMC Biology*   (2023) 21:184

Page 7 of 22

150 µM: this is a realistic high-fat concentration in liver cells, such as under fasting conditions [150, 170]. A large influx of fat to the liver is characteristic of the stress conditions that might precipitate in metabolic decompensation in MCADD [10]. The chain-length distribution of mitochondrial acyl-CoAs at different cytosolic palmitoyl-CoA increments can be seen in Additional File 6: Fig. S2. Simulated patterns of mitochondrial acyl-CoA concentrations recapitulated those of hexanoyl- and octanoylcarnitines in patient crisis urine (Fig. 3). Interestingly, if the metabolite partitioning attribute was removed from the model, the accumulation of C8 and C6 was no longer apparent (Additional File 7: Fig. S3). This suggests that metabolite solubility is important to our understanding of pathogenicity in MCADD.

MCADD could cause severe CoASH depletion

The isoenzymes SCAD and VLCAD catalyse the same reaction as MCAD, but with a preference for shorter or longer acyl-chain lengths, respectively. To get insight into the effects of these different acyl-CoA dehydrogenases (ACADs) on mFAO flux and CoA sequestration, we compared MCAD deficiency to SCAD and VLCAD deficiency.

First, the acyl-CoA profiles of the three human acyl-CoA dehydrogenase deficiencies (ACADDs) were simulated at a high substrate concentration (Fig. 4A). Typical residual activities for symptomatic patients with the respective deficiencies were chosen: 0% activity for MCADD and SCADD [171, 172], and 10% for VLCADD [173]. The acyl-CoA species that accumulated in each disease, matched the substrate preferences of the deficient enzymes: C12, C14 and C16 in VLCADD, C8 in MCADD and C6 and C4 in SCADD. These chain lengths are all known to accumulate as blood acylcarnitines in patients with the corresponding ACAD deficiency [19, 174–178]. mFAO flux was quantified as the rate of production of one of its end products, NADH (Fig. 4B). The SCADD model maintained a residual flux of more than 90% of the control. In contrast, the MCADD model reached a maximum flux of about 60%, and the VLCADD model no more than 30% of control. This reflects the relative severity of the corresponding deficiencies [179–181]. It also highlights one of the strengths of the model, namely that the ACAD isoenzymes with overlapping substrate specificity in part compensate for each other. Consequently, a full ablation of SCAD or MCAD did not entirely block the flux through the pathway.

Figure 4C shows the free, non-esterified mitochondrial CoASH concentration as a function of the concentration of the cytosolic substrate palmitoyl-CoA. All models started with the same amount of CoASH, which decreased sharply as a function of an increasing palmitoyl-CoA concentration. MCADD caused the sharpest decline of CoASH and led to the lowest free CoASH concentration, about 50% of the control model at high palmitoyl-CoA. In the VLCADD model, CoASH remained even higher than in the control model. In VLCADD, the sequestration of CoASH is limited by the fact that the blockage occurs at the beginning of the pathway. First, VLCAD is upstream of MCAD and SCAD. Second, the long-chain acyl-CoA esters that are still formed (Additional File 6: Fig. S2B) cause a strong product inhibition (Additional File 1: Text S1) of the carnitine shuttle, thus limiting the further entry of substrate into the pathway. These effects also contribute to the low flux in VLCADD.

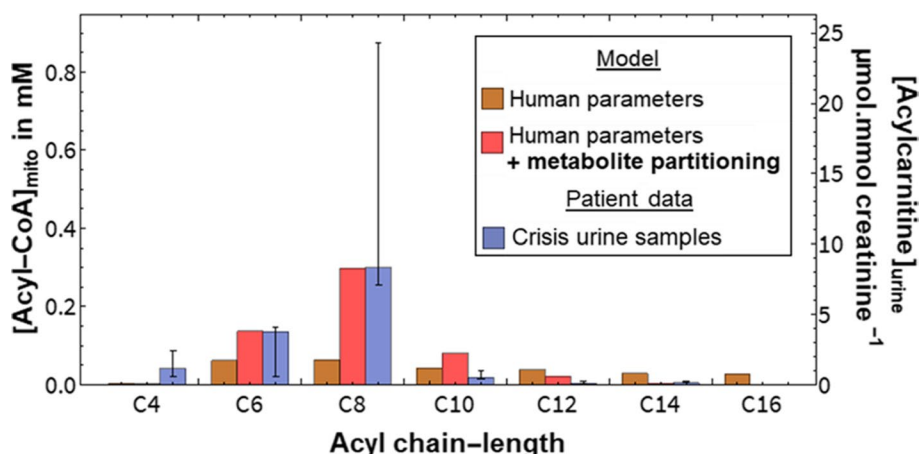The combined results point to a qualitative difference between SCADD, MCADD and VLCADD.

Fig. 3 Patient crisis modelling. Simulated acyl-CoA accumulation in the mitochondrial compartment at 150 µM cytosolic palmitoyl-CoA compared to measured acylcarnitines in the urine of MCADD patients during hypoketotic hypoglycaemia (*n* = 3). The blue bars (measured data, *y*-axis on the right) represent the median and the range of the data (minimum and maximum)
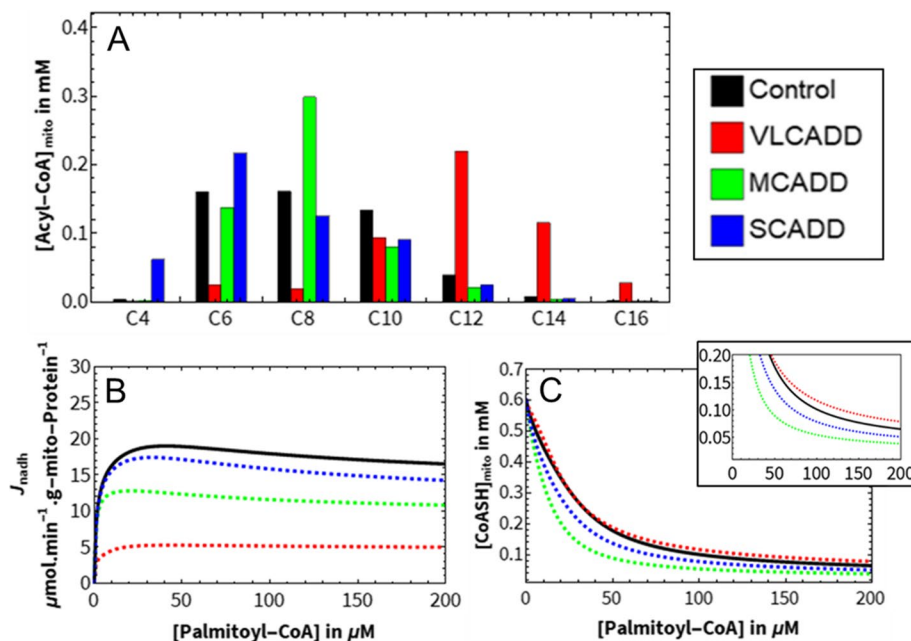
Fig. 4 Comparison of different ACAD deficiencies in silico. The behaviour of one control and three different ACADD computational models of mFAO are shown. The residual activity reflects typical symptomatic patients: 0% for MCADD and SCADD, and 10% for VLCADD. All other ACADs have 100% of control activity. **A** Model mitochondrial acyl-CoA profile at 150 μM cytosolic palmitoyl-CoA. **B** NADH production flux at 150 μM cytosolic palmitoyl-CoA. **C** Steady-state mitochondrial CoASH. Inset gives the same data with a smaller *y*-axis

SCADD and MCADD lead to the accumulation of short- and medium-chain acyl-CoAs, which only weakly inhibit the carnitine shuttle. This permits substrates to continue entering the mitochondrion even at very high acyl-CoA concentrations and thereby allows more extensive sequestration of the CoA pool. One might interpret these results as indicating that MCADD and SCADD are acute CASTOR diseases, MCADD the more severe, in which an increase in substrate concentration can lead to a depletion of CoASH [23]. In MCADD, we see a combination of two effects: a substantial reduction in pathway flux and severe CoASH depletion. In this model, the flux was decreased even if CoASH was set to a constant concentration (Additional File 8: Fig. S4), indicating that the reduced flux is not a consequence of CoASH depletion but simultaneous with it. A model version without metabolite partitioning exhibited no CoASH depletion, milder acyl-CoA accumulations and smaller differences in pathway flux (Additional File 7: Fig. S3).

MCADD poses a threat to mitochondrial metabolism because it simultaneously causes the loss of about 35% of pathway flux relative to the control, as well as a 40% drop in CoASH. This is in contrast to VLCADD, which substantially decreases flux by 70%, but not CoASH. SCADD lowers both, but less strongly than

MCADD (10% flux reduction and 20% CoASH reduction). In our subsequent analyses, we further investigated both of these effects.

Metabolic control analysis identifies possible rescues for MCADD

We hypothesised that clinically asymptomatic MCADD patients may implement compensatory mechanisms that increase pathway flux and CoASH concentration. To identify these, we analysed which enzymes exert a large control over these two model readouts (Fig. 5).

Metabolic control analysis is a theoretical framework that quantifies the sensitivity of the steady-state outputs of a metabolic network to changes in the underlying parameters [139]. Flux control coefficients (Fig. 5A) quantify the percentage change in the flux in response to a 1% increase in enzyme concentration. The flux, again, refers to the rate of NADH production. A positive flux control coefficient means that the flux increases in response to an increased concentration of a given enzyme, while a negative value indicates that flux goes down as the concentration of that enzyme goes up [139]. MTP, VLCAD and MCAD had the largest positive flux control coefficients in the healthy control model, while CPT2 had a large negative flux control coefficient, and the third-highest absolute value
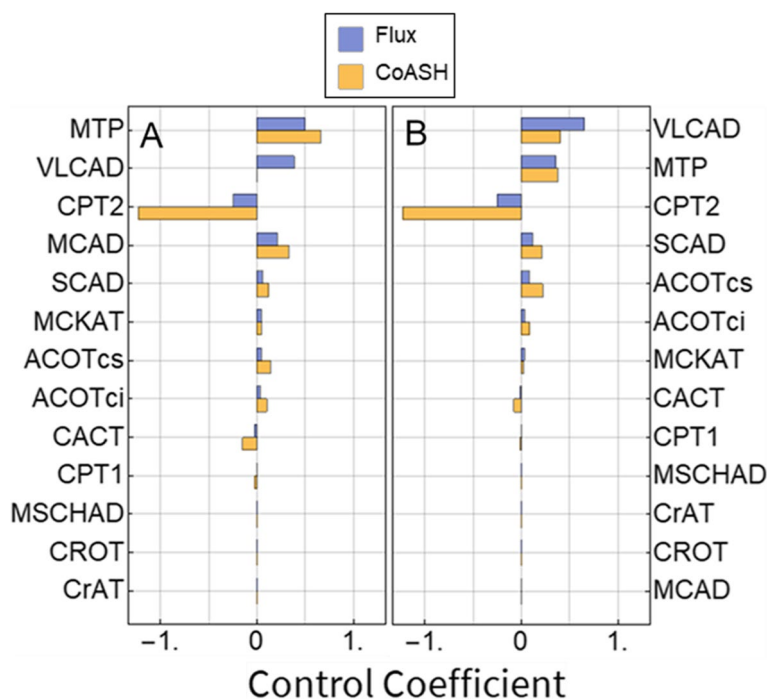
Odendaal *et al. BMC Biology*   (2023) 21:184

Page 9 of 22

Fig. 5 Metabolic control analysis. Flux and mitochondrial CoASH concentration control coefficients (blue and yellow, respectively) in a control (**A**) and an MCADD (**B**) model. Enzymes are displayed in descending order according to absolute flux control. Flux was defined as the sum of all NADH-producing reactions. Simulations were carried out at 150 μM cytosolic palmitoyl-CoA

(Fig. 5A). In the MCADD model, this pattern was the same, except that no flux control coefficient exists for MCAD, leaving SCAD in fourth place and ACOTcs not far behind (Fig. 5A).

Interestingly, CPT1, which is canonically considered the dominant flux-controlling enzyme of the mitochondrial β-oxidation [11], has a very low flux control coefficient in our model. This is in line with other studies, which show that depending on the physiological conditions, control may shift from CPT1 to downstream enzymes [27, 182, 183]. As expected, under conditions of high malonyl-CoA (100 μM), low cytosolic palmitoyl-CoA (2 μM) and abundant free mitochondrial CoA (no sequestration outside mFAO assumed), mitochondrial acetyl-CoA at 120 μM as in fed rats the CPT1 has a much higher FCC (Additional File 9: Fig. S5).

Concentration control coefficients (Fig. 5B) quantify the percentage change in specific steady-state metabolite concentration in response to a 1% increase in enzyme concentration. CPT2 had a large negative concentration control coefficient with respect to the mitochondrial CoASH concentration (Fig. 5B), in both the healthy control and MCADD models. Other enzymes with large flux control coefficients all had large positive concentration control coefficients with respect to the CoASH concentration, except for VLCAD, which

exerted no control at all on CoASH in the healthy control. At a low mitochondrial acetyl-CoA concentration (120 μM; [184]), the concentration control coefficient of VLCAD towards CoASH even became negative (Additional File 10: Fig. S6). Response coefficients (which are calculated in the same way as control coefficients but pertain to all parameters) were also computed for the control model (Additional File 11: Table S3). VLCAD, MTP, CPT2 and MCAD parameters often showed strong responses, as did parameters that directly increase or sequester free CoASH (e.g. total CoA and acetyl-CoA concentration). This sensitivity analysis is consistent with the flux and concentration control coefficients.

Taken together, these results indicate a sensitivity of the pathway flux and CoASH to changes in the levels of CPT2, VLCAD, SCAD, MTP and the ACOTs. For most of these enzymes, increased levels would result in increased CoASH and flux. For CPT2, the relationship is inverted. Most interestingly, VLCAD, which always has a positive flux control, can have either positive or negative control over the CoASH concentration, depending on the conditions at which the analysis is performed. These suggested rescue mechanisms could now serve as candidates for explaining some of the phenotypic heterogeneity between MCADD patients.
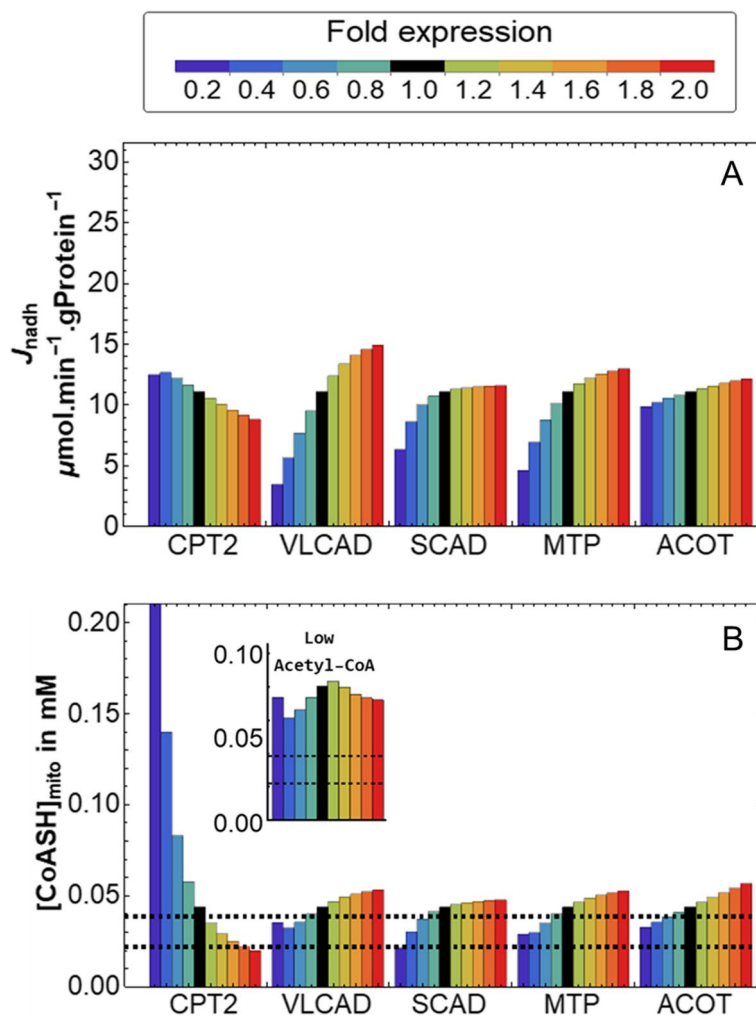
Fig. 6 Possible rescues of CoASH and steady-state mFAO flux in an MCADD model. An MCADD computational mFAO model was simulated at different expression levels of the enzymes identified as possible rescues by metabolic control analysis. The reference value (onefold expression) is given in black. All simulations were performed at 150 μM cytosolic palmitoyl-CoA. The dashed lines in **B** indicate the K_m values of various mitochondrial enzymes that require CoASH as substrate (Table 2). CPT2, VLCAD, SCAD, MTP and ACOT were varied between 20 and 200% of basal expression levels. ACOT was varied by simultaneously increasing the expression of both ACOTs in the model. The inset shows the trajectory of CoASH concentration when VLCAD is incrementally varied with the mitochondrial acetyl-CoA concentration set to 120 μM (lowest value retrieved from literature), compared to the default concentration of 700 μM. **A** NADH production flux. **B** Steady-state mitochondrial CoASH

Increased SCAD, MTP and ACOT could attenuate CoASH depletion and flux decline

A limitation of metabolic control analysis is that it only considers small changes in enzyme activities, while larger changes are required for a substantial rescue. Therefore, six enzymes with high absolute flux or CoASH concentration control in the MCADD model (VLCAD, CPT2, MTP, SCAD, ACOTcs and ACOTci) were varied incrementally from 20 to 200% of their default levels (Fig. 6). The two ACOTs were varied together for simplicity. In agreement with its negative flux control (Fig. 5), decreasing CPT2 increased the pathway flux, while the other enzyme concentrations needed to be increased to get this

effect (Fig. 6A). At the higher SCAD or MTP levels, the flux increase plateaued, as other enzymes took over control. In agreement with its negative CoASH concentration control, decreasing CPT2 increased CoASH, while increasing SCAD, MTP and ACOT, which had positive CoASH concentration control, indeed did increase mitochondrial CoASH (Fig. 6B). In the MCADD model, CoASH (Fig. 6B) was always lower than in the control model (Additional File 12: Fig. S7).

To see what would be the impact of increasing CoASH in the MCADD model, we compared it to the K_m values of mitochondrial enzymes that consume CoASH. These included enzymes of the mFAO but also from the TCA

Table 2 K_m values for CoASH of CoASH-requiring mitochondrial enzymes

Enzyme	Pathway	K_m (mM)	Reference
CrAT	Carnitine shuttle	0.038–0.0888	[86, 91]
MCKAT	mFAO	0.0022–0.0384	[108, 185]
αKDH	TCA cycle	0.0025	[186]
PDH	TCA cycle / glycolysis	0.013–0.025	[186, 187]

cycle (0.0022–0.0888 mM; Table 2 and dashed lines in Fig. 6B). A K_m is an indication of the metabolite concentrations at which an enzyme is most sensitive to concentration changes, so it serves as a guide to where CoASH might become limiting. In the MCADD model, the CoASH concentration varied in the range of the K_m values, implying that even a small increase should have a positive impact on the activity of CoASH-dependent pathways. In comparison, in the control model CoASH concentrations were much higher than the K_m values at any condition (Additional File 12: Fig. S7), implying that changes in the CoASH concentration would have little impact on the activity of these CoASH-consuming enzymes.

In the MCADD model, increasing VLCAD leads to an increase of CoASH (Fig. 6B). However, if the concentration of acetyl-CoA is low (120 µM [184]), increases in VLCAD can cause a reduction in CoASH (inset in Fig. 6B). This may be realistic because a reduced mFAO flux might reduce the acetyl-CoA concentration [29–31]. This suggests a scenario in which increased VLCAD could aggravate CoASH depletion (Table 2).

It may seem surprising that increased ACOT led to consistent flux increases, in both an MCAD (Fig. 6B) and a control (Additional File 12: Fig. S7B) model. Given that ACOTs siphon off pathway intermediates from the β-oxidation, one would expect lower, not higher, NADH production. This suggests that at our chosen simulation conditions CoASH may be limiting or CoA esters might be inhibitory. If CoASH is set to constant levels, increased ACOT decreases flux in the control model but increases it in the MCADD model (Additional File 13: Fig. S8). In the control model, the negative effect of losing pathway intermediates via ACOT seems to dominate. In the MCADD model, however, ACOTs still have a positive effect on pathway flux, although more modest, even if ACOTs do not affect CoASH anymore. We conclude that not only depleted CoASH but also accumulating CoA esters inhibit pathway flux in MCADD. ACOTs alleviate both of these. This is in agreement with the idea that ACOTs modulate acyl-CoA levels and free up CoASH during periods of high substrate influx into the mitochondrion [131, 188].

In summary, the upregulation of SCAD, MTP and the ACOTs, as well as the downregulation of CPT2, were found to have a positive effect on flux and CoASH concentration in MCADD under overload conditions. This renders them potential compensatory mechanisms for mFAO function. A patient with one of these adaptations would be less at risk of a disastrous CoASH depletion than one without them. This is potentially useful information for risk stratification.

Increased SCAD and MTP in a clinically asymptomatic MCADD patient lead to higher flux and CoASH

Proteome remodelling is known to occur in response to enzyme deficiencies [167, 189]. As shown above, certain changes in protein levels could theoretically lead to an increased flux and CoASH. To test whether the corresponding adaptations were recapitulated in real patients, targeted proteomics were measured on fibroblasts from 5 control and 10 MCADD patients [109].

The MCADD patients belonged to different phenotypic groups. The members of the 'control' group are not suspected to have a metabolic disease ($n = 5$). The MCADD patients were all diagnosed before neonatal screening for MCADD was implemented. They were subdivided into three phenotypic subgroups: 'symptomatic' ($n = 4$), i.e. patients that were clinically diagnosed upon admission to hospital with hypoglycaemia; 'early diagnosis' ('ED', $n = 5$), patients that were diagnosed at a young age (0–11 years) as siblings of the symptomatic patients and then put on preventative dietary regimens; and one 'asymptomatic' patient, who was discovered as an adult (30 years) and never exhibited clinical symptoms nor received treatment ($n = 1$).

As expected, cells from MCADD patients had undetectable MCAD protein levels, in contrast to those from the control group (Additional File 14: Fig. S9, original data available at [190]). The other protein concentrations of symptomatic and ED patients did not differ significantly from each other, nor from the control group. Table 3 shows the average protein concentrations of the asymptomatic patient, of all groups together, and of the MCADD groups together (all excluding controls). The asymptomatic patient had the highest average SCAD level out of any of the subjects (Fig. 7A). Moreover, the asymptomatic patient's SCAD was above the upper limit of the 95% confidence interval when all subjects were combined into one group (Table 3). This was not the case for any other peptide. The two subunits of MTP (HADHa and HADHb) were at the higher end of the concentration range in the asymptomatic patient (Fig. 7A), but still within the confidence interval. CPT2's concentration did not differ between the asymptomatic patient and the

Odendaal *et al. BMC Biology*   (2023) 21:184

Page 12 of 22

Table 3 Peptide concentrations per group (fmol.µg-total-protein^{-1})

Peptide	Asymptomatic	All subjects (n = 14)	All MCADD (n = 10)
	Mean (95% confidence intervals, based on t distribution)		
CPT2	0.21	0.19 (0.09–0.29)	0.19 (0.10–0.28)
VLCAD	1.60	1.33 (0.30–2.36)	1.41 (0.44–2.38)
MCAD	0.23	0.52 (-0.65–1.68)	0.18 (0.06–0.29)
SCAD	0.38	0.21 (0.06–0.37)	0.21 (0.04–0.38)
ETFa	0.36	0.32 (0.14–0.50)	0.34 (0.13–0.54)
ETFb	1.03	1.09 (0.37–1.81)	1.12 (0.37–1.81)
MCKAT	2.84	2.68 (0.53–4.83)	2.71 (0.58–4.83)
HADHa	1.80	1.34 (0.57–2.10)	1.41 (0.64–2.17)
HADHb	1.80	1.26 (0.35–2.18)	1.29 (0.39–2.20)

other subjects in the cohort. ACOT was not included in the applied proteomics panel.

The computational mFAO model was then personalised using the proteomics data and fluxes and CoASH concentrations simulated per person. To this end, the V_{max} of each of the enzymes was multiplied by the corresponding enzyme concentration in an individual relative to that of the average control. This yielded a model of the liver mFAO in each individual patient. First and foremost, the asymptomatic patient model had a higher pathway flux than all the symptomatic MCADD patient models. None of the other groups differed significantly from each other in terms of flux, including the control group. The mitochondrial CoASH of all MCADD models differed from that of the control models ($p = 0.080$ with the asymptomatic patient model included; $p = 0.061$ when excluded), suggesting a trend that might be validated with a larger sample size. In addition, the asymptomatic patient model showed higher CoASH than all symptomatic MCADD models (Fig. 7B, C), even reaching the range seen in the healthy control models. Since the CoASH concentrations remain close to the K_m values of CoASH-dependent enzymes in the mitochondrion (Table 2), this elevated CoASH concentration in the asymptomatic patient is likely to have a stimulatory effect on CoASH-dependent reactions.

If we hypothesise that flux decline and CoASH depletion contribute to the development of hypoketotic hypoglycaemia, then our results suggest that altered expression of genes encoding for SCAD and MTP has contributed to the lack of symptoms in the asymptomatic patient. The ED patients did not show such adaptations. Of course, the model is blind to adaptations outside its included reactions, such as in gluconeogenesis or ketogenesis, and to changes in the pathway kinetics due to post-translational modifications like acetylation [191]. TCA cycle enzymes and selected respiratory chain subunits were included in the proteomics, but were not altered in any of the MCAD groups compared to the controls (Additional File 14: Figure S9). Alternatively, the lack of symptoms in ED patients may be due to their early detection and subsequent dietary advice, which might have interfered with the natural disease development.

Finally, the availability of fibroblast proteomics from only a single clinically certain asymptomatic individual complicates the statistical interpretation of the personalised model predictions. The limited availability of patients in this category is due to the rarity of the disease and the early detection by newborn screening, which was introduced in 2007 [19]. We are dependent on historical samples, as interventions introduced after detection by newborn screening can interfere with natural disease progression. This is in line with the development of so-called 'N of 1' trials for rare diseases [192], which may in the future also benefit from computational models. We could partially address the lack of asymptomatic replicates by comparing the results of the asymptomatic individual to the confidence intervals belonging to other clinical groups.

Towards the digital twin

We have shown how a kinetic model can be used to investigate the pathophysiology of an inborn error of metabolism (IEM). It can not only be used to identify theoretical sources of phenotypic heterogeneity but— together with phenotypical knowledge—it can also be personalised to predict individual phenotypes. In this respect, kinetic models are complementary to genome-scale metabolic models (GEMs; [193, 194]). In contrast to the latest version of the GEM Recon3D [154], which maps more than 230 IEMs, kinetic models focus on specific pathways and contain fewer enzymes and reactions. For this study, however, a kinetic model is better suited, as it allows the explicit simulation of metabolite concentrations and the phenomenon of sequestration of CoA in acyl-CoA esters [25, 27]. Metabolite partitioning can also be intuitively included into a model with explicit metabolite concentrations. Also, the compensatory role of SCAD in MCADD is better represented by a kinetic model, since it depends on the relative affinities of the enzymes for their substrates, as quantified by the K_m values. Steps have been taken towards enzyme-constrained
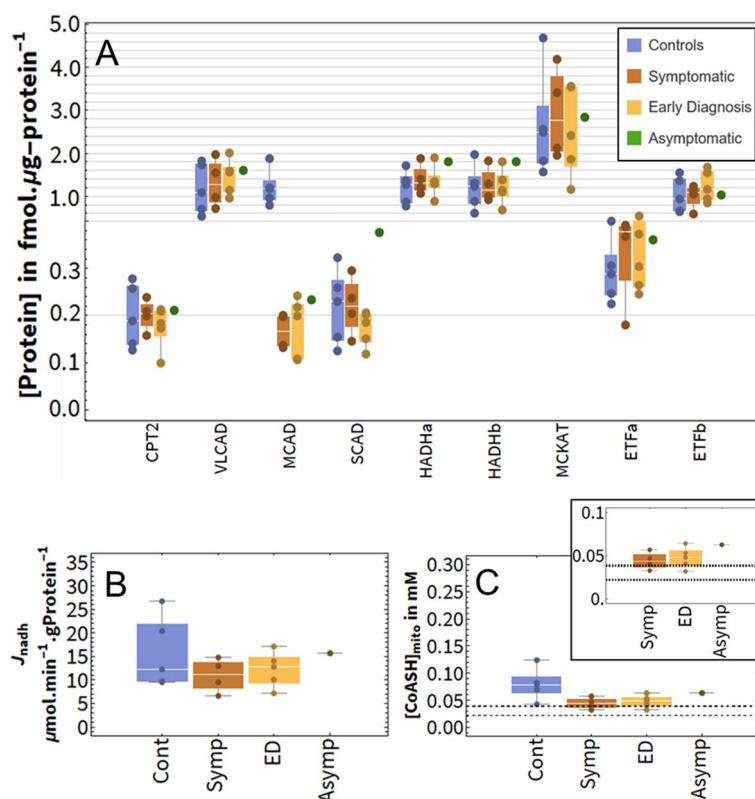
Fig. 7 Steady-state mFAO flux and mitochondrial CoASH in personalised patient models. Fibroblasts proteomics from four phenotypic groups were used to personalise the kinetic model of mFAO: *Controls* ($n=5$), *symptomatic* ($n=4$), *early diagnosis*, (*ED*, $n=5$) and *asymptomatic* ($n=1$). All simulations were done at 150 µM cytosolic palmitoyl-CoA. **A** Normalised, measured expression of key β-oxidation proteins per clinical group. Individual people are averages of at least three technical replicates and are represented as data points in the distribution bars. HADHa and HADHb are the two subunits of MTP. **B, C** Simulation results from personalised computational models: flux and mitochondrial CoASH concentration. Dashed lines indicate the region of the $K_{m,CoASH}$ values of key mitochondrial enzymes: PDH, αKDH, MCKAT and CrAT (Table 2). Control and MCADD were compared using a *t*-test

GEM models, incorporating some of the detail of kinetic models into large networks [193].

The use of personalised computational models to stratify patients requires that these models become increasingly accurate and comprehensive. This highlights the importance of systematically measuring and reporting enzyme kinetics—an endeavour which is facilitated by databases and consortia such as SABIO-RK and STRENDA DB [195, 196]. Advances in enzymology will help to further establish accurate kinetic descriptions of individual reactions, leading to more clinically relevant computational models.

A limitation of this study is that the model only comprises the mitochondrial fatty acid oxidation. An extension of the model with gluconeogenesis, TCA cycle and ketogenesis would introduce an explicit link to the clinical phenotype of hypoketotic hypoglycaemia [29–31, 33, 34]. In an extended model, we expect that the decline of the fatty acid oxidation flux reduces the production of ATP as an important source of Gibbs energy

for gluconeogenesis and the production of acetyl-CoA as a precursor for ketogenesis. Moreover, the depletion of CoASH would directly impact other enzymes that require this cofactor. Another important extension could be fatty acid oxidation in peroxisomes and microsomes [197]. The peroxisome can take over the oxidation of some straight long- and medium-chain fatty acids when the mFAO is impaired [198]. Moreover, this extension would make a direct link to diagnostic markers of MCADD, such as dicarboxylic acids [19, 168] and glycine conjugates of fatty acids [19, 168].

Many factors may contribute to phenotypic heterogeneity among people with mFAO disorders, including genetic, post-translational, and environmental differences [2, 3, 199–202]. We considered one of these sources of heterogeneity—changes in enzyme concentrations—and incorporated it into a computational model. This type of personalisation relies on the availability of patient-specific proteomics. Improved measurement techniques and patient-specific in vitro models are

Odendaal *et al. BMC Biology*   (2023) 21:184

Page 14 of 22

important for this. Recent advances in targeted proteomics have allowed for increasingly accurate quantification of the proteome, also from human cells [203–205]. Here we used the QConCAT technology to generate ^{13}C-lysine and -arginine labelled peptide standards [109]. The advantage of this method is not only the efficient generation of many standards together but also that it allows to correct for the loss of protein during sample treatment. The limitation is, however, that the set of measured proteins is predetermined and cannot be flexibly adapted. Here, for instance, analysis of the various ACOTs would have been of interest, but these are not present in the applied mitochondrial panel. With respect to in vitro models, this study was based on fibroblast proteomics, but ideally, a computational model of liver metabolism would be personalised with liver proteomics. Since direct biopsies from patient livers are too invasive, more representative in vitro models of MCADD patients and other IEM patients have to be generated. One promising way forward is the generation of induced pluripotent stem cells (iPSCs) from cells collected in less invasive ways, like fibroblasts from skin grafts [206]. These iPSCs can be differentiated into liver organoids, which, if cultured under appropriate physiological conditions, would be a better representation of a native liver [207–210]. A limitation of current hepatic organoid cultures is, however, that they produce little or no glucose, and therefore lack an important clinical readout [211–213]. Finally, the patient fibroblasts used in this study were historical, which complicated phenotypical assessment, since the conditions that triggered metabolic crisis were obviously not controlled. Controlled clinical human studies, such as the Fasting Tolerance in MCADD Infants study [214], are necessary to generate (patho)physiologically relevant patient data under standardised conditions and to increase the statistical power of personalised modelling.

Eventually, advances in personalised kinetic modelling hold the promise of increasingly accurate in silico representations of individual patients. Such 'digital twins' of increasing scope and complexity [5, 7, 8] would capture the interaction of a pathogenic mutation embedded within the biochemical networks that determine the trajectory of disease development [3, 215]. This would allow researchers to non-invasively simulate patient outcomes under a variety of perturbations. These simulations would aid in diagnosis, prognosis and predictions of treatment efficacy in a precise and person-specific way.

Conclusions

In this paper, we presented—to our knowledge—the first computational, kinetic model of mFAO in human liver, and certainly, the first in which differential metabolite localisation due to differences in water solubility has been explicitly addressed. Model simulations identified the risk of a simultaneous reduction in pathway flux and a depletion of CoASH in MCADD. In theory, upregulation of SCAD, MTP and/or the ACOTs are possible rescues to preserve pathway flux and CoASH. Indeed, proteomics analysis of individual patients' cells revealed the upregulation of SCAD and MTP in an asymptomatic patient. This was also the first time that patient data were directly employed to personalise computational models for the investigation of MCADD. Increased SCAD as a rescue for MCADD has also not been explicitly reported before. Altogether, this study shows the potential and direction of personalised computational modelling for unravelling disease evolution, stratifying risk among patients, and, in future, testing interventions.

Methods

Generation of HepG2 MCAD-KO cell line

ACADM was knocked out in HepG2 cells (order number: ATCC-HB-8065, ATCC, Manasses, Virginia, USA) by CRISPR-Cas9, with guide sequence 5′-GGGGTT CGGGCGATGCTGCA-3′, which was designed using the online CRISPR Design Tool [216]. The sequence of the T7 promoter is added 5′ of the guide sequence and additional nucleotides are included for cloning into a pX459 vector (pSpCas9(BB)-2A-Puro) [164]. These oligonucleotides were ordered from Invitrogen (Waltham, Massachusetts, USA). Correct insertion was confirmed by Sanger sequencing (GATC Biotech, Ebersberg, Germany). The HepG2 cells were transfected with the sgRNA-coding plasmids using Lipofectamine 3000 according to the manufacturer's instructions [217].

Human fibroblasts

Fibroblasts of patients without a documented heritable metabolic disease (*n* = 5; *control*) and fibroblasts of patients with MCADD were obtained from the Department of Genetics of the University Medical Centre Groningen. All patients with MCADD were homozygous for c.985A > G missense mutation in the *ACADM* gene and were born before neonatal screening for MCADD was implemented in the Netherlands (< 2007). Three subgroups were distinguished. *Symptomatic* (*n* = 4), patients that suffered from at least one recorded metabolic crisis leading to hospitalisation with hypoglycaemia (< 2.6 mmol/L), coma and/or seizures (*n* = 4). *Early diagnosis* individuals (*n* = 5; abbreviated *ED*), siblings of the symptomatic patients who were diagnosed during proband follow-up (ages 0–11 years), were detected and subsequently received preventative dietary advice. *Asymptomatic* (*n* = 1) was discovered well into adulthood (30 years of age), without having ever had noticeable

symptoms. Case characteristics are given in Additional File 15: Table S4.

Genotyping

Genomic DNA was isolated and part of the MCAD gene was amplified by PCR using forward (CTGGCAGCT CTTCTCAAAGC) and reverse (TTCAAGGAGTAG CTGCTC) primers. The PCR product of 350 bp was subcloned into pZERO-blunt and at least 7 colonies per cell line were genotyped by Sanger sequencing.

Immunoblotting

Western blotting was performed according to a previously described method [218]. GAPDH was used as a positive control. Commercially available antibodies were used to detect GAPDH (AB8245, Abcam, Cambridge, UK) and MCAD (AB92461, Abcam, Cambridge, UK). The original images can be found in Additional File 16: Fig. S10.

Proteomics

Concentrations of mFAO enzymes and carrier proteins were quantified by liquid chromatography coupled to mass spectrometry in selected reaction monitor mode (LC–MS-SRM), with ^{13}C-lysine and -arginine labelled QConCATs targeting a panel of mitochondrial proteins according to [109].

Acylcarnitine analysis in MCADD patients' urine

Seven MCADD patients were included, all of whom were homozygous for the c.985A > G missense mutation in the *ACADM* gene and identified before the introduction of MCADD to the Dutch newborn screening. The median age at inclusion was 29 years (range 14–76). The MCADD patients were retrospectively categorised as symptomatic (*n* = 3) or asymptomatic (*n* = 4) according to the same criteria used for the patient fibroblasts. For all patients, acylcarnitines were measured according to Derks et al. [176] in urine obtained after an overnight fast (*fasting*), and in the first urine after breakfast (*fed*). For the symptomatic patients, historic urine samples taken during a first metabolic derangement (at ages 11–13 months) (*crisis*) were retrieved from storage (stored at − 80 °C) and measured.

Informed consent

For the use of patient urine for the measurement of acylcarnitines, written consent was obtained.

For the use of historical patient fibroblasts, the Medical Ethical Committee of the University Medical Centre Groningen confirmed that according to Dutch law, the Medical Research Involving Human Subjects Act (WMO) does not apply to this study and that an official approval by the Ethical Committee was not required (METc 2016/590).

Cell culture

Cell cultures were kept at 37 °C and 5% CO_2. Wild-type and MCAD-KO HepG2 cells were cultured in Dulbecco's modified Eagle's medium with 1 g.L^{-1} glucose, 3.7 g.L^{-1} NaHCO$_3$, 0.11 g.L^{-1} sodium pyruvate, and amino acids (catalogue number P04-01500, PAN Biotech™, Aidenbach, Germany) with glutamine and NaCl added to a final concentration of 3 mM, supplemented with 10% foetal calf serum (FCS, Gibco™). Assays were performed only on cells that had been passaged fewer than 20 times. Human fibroblasts were cultured in Ham's F-10 Nutrient Mix (Thermo Fisher Scientific 11550,043), supplemented with 10% foetal calf serum (FCS, Gibco™), 1% penicillin/ streptomycin (PenStrep, Gibco™). Seventy-two hours before harvesting the cells, the medium was changed and supplemented with 0.4 mmol.L^{-1} L-carnitine.

High-resolution respirometry

HepG2 cells were detached by trypsinisation (0.25% Trypsin–EDTA, Gibco™). After 10 min, the trypsin was inactivated by washing with cell culture medium containing 10% FCS. O_2 consumption flux was then measured in a miRO5 buffer containing 25 μM palmitoyl-CoA, 2 mM L-carnitine and 2 mM malate as the substrates, using an Oroboros Oxygraph-2 k (O2k, Oroboros Instruments, Austria) as described by Van Zutphen et al. [219]. Instead of an ADP-generating system, we directly added 1 mM of ADP. For normalisation to cellular protein, cells were sonicated twice at 20 kHz, 40% amplitude for 30 s (VCX130, Sonics & Materials Inc., Newton, CT., USA). Protein was quantified in the lysate with the BCA protein assay kit (Pierce, Thermo Fisher Scientific Inc., Rockford, IL., USA). Each point in the data set represents one biological repeat.

Computational model

Model construction and analysis were performed in Wolfram Mathematica version 12.1. Ordinary differential equations (ODEs) were solved with the NDSolve function. Steady states were then calculated by the Newton–Raphson method as the point at which the time derivatives in all ODEs equalled zero (FindRoot function with *MaxIterations—> Infinity*), with the end point of the time evolution as an initial guess. All inspected steady states fulfilled the criterion that time derivatives were close to zero ($< 10^{-10}$). Varying the initial metabolite concentrations did not result in alternative steady states. Where metabolic control analysis (MCA) was performed, the summation theorem was satisfied in all cases, confirming the internal consistency of the analysis. Thus, the sum of all flux control coefficients equals unity and the sum of all concentration control coefficients equals zero [139]:

Table 4 Personalised parameters based on fibroblast proteomics data

Phenotype Unit	Person	$V_{max,VLCAD}$	$V_{max,MCAD}$[a]	$V_{max,SCAD}$[b]	$V_{max,MCKAT}$	$V_{max,MTP}$	Total ETF
		\multicolumn{5}{l}{μmol.min^{-1}.mg-mitochondrial-Protein^{-1}}			μM
Default		0.076	0.038	0.01668	2.98	0.167	46.0
Control	C103	0.042	0.037	0.01668	2.82	0.178	27.4
	C104	0.066	0.025	0.01668	1.78	0.088	39.8
	C105	0.104	0.059	0.01668	5.32	0.243	65.2
	C106K	0.110	0.030	0.01668	2.92	0.187	57.5
	C106W	0.032	0.038	0.01668	2.07	0.122	28.0
Symptomatic	P1	0.044	0	0.01668	2.41	0.132	24.7
	P5	0.118	0	0.01668	2.22	0.145	48.0
	P7	0.059	0	0.01668	4.74	0.181	44.5
	P8	0.094	0	0.01668	3.88	0.258	52.5
Early diagnosis	P2	0.069	0	0.01668	2.73	0.159	39.4
	P3	0.058	0	0.01668	1.32	0.097	35.7
	P4	0.121	0	0.01668	4.02	0.252	65.7
	P6	0.094	0	0.01668	4.03	0.193	70.8
	P9	0.096	0	0.01668	2.12	0.166	48.9
Asymptomatic	P10	0.096	0	0.02776	3.22	0.257	43.6

[a] $V_{max,MCAD}$ activity was set to zero in all MCADD patients

[b] $V_{max,SCAD}$ was set to the default value for all patients except P10, since the measurements were too close to the limit of detection to be precisely quantified. For P10, however, the SCAD concentration could be concluded to differ from the other persons in the cohort and was adapted

$$\sum_i \text{Flux control coefficient}_i = 1$$

$$\sum_i \text{Concentration control coefficient}_i = 0$$

A detailed model description is included in Additional File 1: Text S1. In keeping with FAIR data practices, the model is available on the repository JWS Online Biological Systems Modelling [220]. The model can be viewed, downloaded and simulated directly via on JWS Online [221].

To simulate metabolic stress that could lead to a metabolic crisis, the cytosolic palmitoyl-CoA concentration was set to 150 μM, which is approximately the highest concentration of liver cytosolic long-chain acyl-CoAs reached in vivo [150]. All other parameters were set to their default values (Additional File 1: Text S1) unless otherwise noted.

Personalised models of individual patients

To transform the generic model of human mFAO into personalised models, we made use of the property that the maximal catalytic activity (V_{max}) of a protein is proportional to its concentration. The V_{max} values in the model were retrieved directly from the literature, while the underlying protein concentration was not explicitly quantified. In model personalisation, the mean protein concentration of the control fibroblasts was chosen as the reference value, effectively equal to the implicit protein concentration underlying the model's V_{max} values. The measured protein concentration of each enzyme in an individual's fibroblasts was normalised to the corresponding reference ($^{[E]_{person}}/_{[E]_{controlmean}}$). The default V_{max} values (and the ETF concentration) in the default model were multiplied by this relative fibroblast protein concentration to yield the personalised parameters (Table 4). Proteins that could not be quantified were set to control levels.

Statistical methods

The grouped fluxes and mitochondrial CoASH concentrations from the personalised models were compared using Student's two-tailed *t*-test. Before performing the test, the normality of the data was inspected using a quantile–quantile plot. This was done for all phenotypic groups, as well as for the phenotypically grouped MCADD models grouped.

Abbreviations

IEM	Inborn error of metabolism
mFAO	Mitochondrial fatty acid β-oxidation
CASTOR	Coenzyme A sequestration, toxicity and redistribution
CoASH	Free coenzyme A
MCAD	Medium-chain acyl-CoA dehydrogenase
MCADD	MCAD deficiency
ED	Early diagnosis
CPT1	Carnitine palmitoyltransferase 1

CPT2	Carnitine palmitoyltransferase 2
CACT	Carnitine acylcarnitine translocase
VLCAD	Very-long-chain acyl-CoA dehydrogenase
SCAD	Short-chain acyl-CoA dehydrogenase
ACAD	Acyl-CoA dehydrogenase
CROT	Crotonase
M/SCHAD	Medium-/short-chain hydroxyacyl-CoA dehydrogenase
MCKAT	Medium-chain ketoacyl-CoA thiolase
MTP	Mitochondrial trifunctional protein
ACOTcs	Acyl-CoA thioesterase (CoA-sensitive)
ACOTcs	Acyl-CoA thioesterase (CoA-insensitive)
ETF	Electron-transferring flavoprotein

Supplementary Information

The online version contains supplementary material available at https://doi.org/10.1186/s12915-023-01652-9.

Additional file 1: Text S1. Model description. Description of the model, its underlying assumptions, a list of its variables, rate equations, ordinary differential equations, parameters, conserved moieties, and initial conditions.

Additional file 2: Text S2. Model validation assumptions and calculations. The assumptions and calculations applied to relate the model predictions to measured data for validation purposes.

Additional file 3: Table S1. Sanger Sequencing HepG2. Results of genotyping WT HepG2 cells and four MCAD-knockouts.

Additional file 4: Figure S1. Confirmation of MCAD-knockout. Western blotting and targeted proteomics.

Additional file 5: Table S2. Full patient urine acylcarnitine profiles. Historical urine acylcarnitine data from symptomatic and asymptomatic MCADD patients.

Additional file 6: Figure S2. The simulated effect of MCADD on the acylation of CoA in the mitochondrion. Representation of the amount of the CoA pool that is free, or sequestered as acyl-CoAs of various chain lengths.

Additional file 7: Figure S3. The effect of different ACAD deficiencies in silico without metabolite partitioning. NADH production flux and mitochondrial CoASH concentration as a function of cytosolic palmitoyl-CoA concentration with metabolite partitioning removed.

Additional file 8: Figure S4. The effect of different ACAD deficiencies in silico with fixed mitochondrial CoASH. NADH production flux and mitochondrial CoASH concentration as a function of cytosolic palmitoyl-CoA concentration with a constant CoASH of 600 μM.

Additional file 9: Figure S5. Control analysis at low substrate, high malonyl-CoA concentrations, control MCAD activity. Metabolic control analysis showing a case where CPT1 has the highest flux control.

Additional file 10: Figure S6. Control analysis at low acetyl-CoA. Metabolic control analysis showing high VLCAD flux control but negative CoASH concentration control.

Additional file 11: Table S3. Full sensitivity analysis. Flux and CoASH concentration response coefficients for all model parameters at [palmitoyl-CoA] = 10 μM and 150 μM.

Additional file 12: Figure S7. Effect of possible rescues of mitochondrial CoASH and steady-state mFAO flux in a control model. Effect of incremental changes in VLCAD, SCAD, MTP, ACOT, and CPT2 in a control model activity on NADH flux and CoASH concentration.

Additional file 13: Figure S8. Possible rescues of steady-state mFAO flux in an MCADD model with fixed mitochondrial CoASH. Effect of incremental changes in VLCAD, SCAD, MTP, ACOT, and CPT2 activity with a constant CoASH of 600 μM on NADH flux in a control and MCADD model.

Additional file 14: Figure S9. Protein concentration per technical replicate. Concentration of mFAO proteins in MCADD and control fibroblasts.

Additional file 15: Table S4. Overview of patient characteristics. ID, sex, categorisation, age of onset/diagnosis, and description of MCADD and control individuals from whom fibroblasts were taken.

Additional file 16: Figure 10. Western blots for confirming MCAD-KO. Unedited, uncropped Western blots used to confirm the absence of MCAD in the MCAD-KO cell lines.

Authors' contributions

CO and EAJ jointly wrote the manuscript, interpreted the data and created all figures and tables with input from MAVL, AMFM, NCAH, LAK, JCW, KvE, TGJD and BMB. CO constructed the computational model and carried out all simulations. CO and AG performed the high-resolution respirometry assays. EAJ identified and retrieved patient and control fibroblasts and crisis urine samples from the UMCG's biobank. EAJ and AMFM cultured fibroblasts and prepared samples for proteomics. CO performed the targeted proteomics and assisted in the interpretation of the data. RH-F performed the acylcarnitine measurements on urine samples. MAVL, AMFM, LAK and NCAH generated and confirmed the HepG2 MCAD knockout. AMFM contributed substantially to model construction and ideation in the early stages of the study. MAVL checked the reproducibility of the model. KvE was a major contributor in writing the manuscript and interpreting all data. BMB and TGJD conceived and supervised the study. All authors ready and approved the final manuscript.

Availability of data and materials

All data generated or analysed during this study are included in this published article, its supplementary information files, and publicly available repositories. The datasets supporting the conclusions of this article are available on the FAIRDOM Hub repository [190]. SBML files of models can be downloaded from and simulated on the JWS Online model repository [160, 161, 221].

Declarations

Ethics approval and consent to participate
Written informed consent was obtained from patients participating in the urinary acylcarnitine study. The use of historical patient fibroblasts was approved for waived consent (METc 2016/590).

Consent for publication
Not applicable.

Competing interests
The authors declare that they have no competing interests.

Author details
[1]Laboratory of Paediatrics, University of Groningen, University Medical Centre Groningen, Groningen, the Netherlands. [2]Section of Metabolic Diseases, Beatrix Children's Hospital, University of Groningen, University Medical Centre Groningen, Groningen, the Netherlands. [3]Department of Laboratory Medicine, University of Groningen, University Medical Centre Groningen, Groningen, the Netherlands.

References

1. Ferreira CR, Rahman S, Keller M, Zschocke J. An international classification of inherited metabolic disorders (ICIMD). J Inherit Metab Dis. 2021;44(1):164–77.
2. Vockley J. Metabolism as a complex genetic trait, a systems biology approach: Implications for inborn errors of metabolism and clinical diseases. J Inherit Metab Dis. 2008;31(5):619–29.
3. Argmann CA, Houten SM, Zhu J, Schadt EE. A next generation multiscale view of inborn errors of metabolism. Cell Metab. 2016;23(1):13–26.
4. Hornberg JJ, Bruggeman FJ, Westerhoff HV, Lankelma J. Cancer: a systems biology disease. BioSystems. 2006;83(2–3 SPEC. ISS):81–90.
5. Subramanian K. Digital twin for drug discovery and development—the virtual liver. J Indian Inst Sci. 2020;100(4):653–62.
6. Snoep JL. The Silicon Cell initiative: Working towards a detailed kinetic description at the cellular level. Curr Opin Biotechnol. 2005;16(3 SPEC. ISS.):336–43.
7. Kamel Boulos MN, Zhang P. Digital twins: from personalised medicine to precision public health. J Pers Med. 2021;11(8):745.
8. Cedersund G, Herrgårdh T. eHealth 3.0 : Personalized digital twins to capture and use different kinds of clinical knowledge. In: International Symposium on Health Information Management Research. 2020. p. 4–5.
9. Schatz UA, Ensenauer R. The clinical manifestation of MCAD deficiency: challenges towards adulthood in the screened population. J Inherit Metab Dis. 2010;33(5):513–20.
10. Vockley J, Bennett M, Gillingham M. Mitochondrial fatty acid oxidation disorders. In: Beaudet A, Vogelstein B, Kinzler K, editors. OMIM. New York: The McGraw-Hill Companies; 2014.
11. Eaton S. Control of mitochondrial β-oxidation flux. Prog Lipid Res. 2002;41(3):197–239.
12. Iafolla AK, Thompson RJ, Roe CR. Medium-chain acyl-coenzyme A dehydrogenase deficiency: clinical course in 120 affected children. J Pediatr. 1994;124(3):409–15.
13. Derks TGJ, Reijngoud DJ, Waterham HR, Gerver WJM, van den Berg MP, Sauer PJJ, et al. The natural history of medium-chain acyl CoA dehydrogenase deficiency in the Netherlands: clinical presentation and outcome. J Pediatr. 2006;148(5):665–70.
14. Derks TGJ, Van Spronsen FJ, Rake JP, Van Der Hilst CS, Span MM, Smit GPA. Safe and unsafe duration of fasting for children with MCAD deficiency. Eur J Pediatr. 2007;166(1):5–11.
15. Dixon M, Champion M. Medium chain acyl CoA dehydrogenase deficiency: dietary management guidelines for dietitians. British Inherited Metabolic Disease Group. 2008. https://e-lactancia.org/media/papers/MCADD-dietitiansguidelines-2009.pdf. [Cited: 2023-08-21].
16. Walter JH. Tolerance to fast: rational and practical evaluation in children with hypoketonaemia. J Inherit Metab Dis Off J Soc Study Inborn Errors Metab. 2009;32(2):214–7.
17. Spiekerkoetter U, Bastin J, Gillingham M, Morris A, Wijburg F, Wilcken B. Current issues regarding treatment of mitochondrial fatty acid oxidation disorders. J Inherit Metab Dis. 2010;33(5):555–61.
18. Tanaka K, Yokota I, Coates PM, Strauss AW, Kelly DP, Zhang Z, et al. Mutations in the medium chain acyl-CoA dehydrogenase (MCAD) gene. Hum Mutat. 1992;1:271–9.
19. Jager EA, Kuijpers MM, Bosch AM, Mulder MF, Gozalbo ER, Visser G, et al. A nationwide retrospective observational study of population newborn screening for medium-chain acyl-CoA dehydrogenase (MCAD) deficiency in the Netherlands. J Inherit Metab Dis. 2019;42(5):890–7.
20. Wilson CJ, Champion MP, Collins JE, Clayton PT, Leonard JV. Outcome of medium chain acyl-CoA dehydrogenase deficiency after diagnosis. Arch Dis Child. 1999;80(5):459–62.
21. Karaceper MD, Chakraborty P, Coyle D, Wilson K, Kronick JB, Hawken S, et al. The health system impact of false positive newborn screening results for medium-chain acyl-CoA dehydrogenase deficiency: a cohort study. Orphanet J Rare Dis. 2016;11(1):1–9.
22. Morrison DR, Clayton EW. False positive newborn screening results are not always benign. Public Health Genomics. 2011;14(3):173–7.
23. Mitchell GA, Gauthier N, Lesimple A, Wang SP, Mamer O, Qureshi I. Hereditary and acquired diseases of acyl-coenzyme A metabolism. Mol Genet Metab. 2008;94(1):4–15.
24. Yang H, Zhao C, Wang Y, Wang SP, Mitchell GA. Hereditary diseases of coenzyme A thioester metabolism. Biochem Soc Trans. 2019;47(1):149–55.
25. van Eunen K, Volker-Touw CML, Gerding A, Bleeker A, Wolters JC, van Rijt WJ, et al. Living on the edge: substrate competition explains loss of robustness in mitochondrial fatty-acid oxidation disorders. BMC Biol. 2016;14(1):1–15.
26. van Eunen K, Simons SMJ, Gerding A, Bleeker A, den Besten G, Touw CML, et al. Biochemical competition makes fatty-acid β-oxidation vulnerable to substrate overload. PLoS Comput Biol. 2013;9(8):2–9.
27. Martines ACMF, van Eunen K, Reijngoud DJ, Bakker BM. The promiscuous enzyme medium-chain 3-keto-acyl-CoA thiolase triggers a vicious cycle in fatty-acid beta-oxidation. PLoS Comput Biol. 2017;13(4):1–22.
28. Fletcher JA, Deja S, Satapati S, Fu X, Burgess SC, Browning JD. Impaired ketogenesis and increased acetyl-CoA oxidation promote hyperglycemia in human fatty liver. JCI Insight. 2019;4(11):e127737.
29. McGarry JD, Foster DW. The regulation of ketogenesis from octanoic acid. The role of the tricarboxylic acid cycle and fatty acid synthesis. J Biol Chem. 1971;246(4):1149–59.
30. Perry RJ, Peng L, Cline GW, Petersen KF, Shulman GI. A non-invasive method to assess hepatic acetyl-CoA in vivo. Cell Metab. 2017;25(3):749–56.
31. Foster DW. The role of the carnitine system in human metabolism. Ann N Y Acad Sci. 2004;1033:1–16.
32. Williamson JR, Browning ET, Scholz R, Kreisberg RA, Fritz IB. Inhibition of fatty acid stimulation of gluconeogenesis by (+)-decanoylcarnitine in perfused rat liver. Diabetes. 1968;17(4):194–208.
33. Kunji ERS, Aleksandrova A, King MS, Majd H, Ashton VL, Cerson E, et al. The transport mechanism of the mitochondrial ADP/ATP carrier. Biochim Biophys Acta - Mol Cell Res. 2016;1863(10):2379–93.
34. Berg JM, Tymoczko JL, Gatto GJ, Stryer L. Glycolysis and gluconeogenesis. In: Berg JM, Tymoczko JL, Gatto GL, Stryer L, editors. Biochemistry. 8th ed. New York: W.H. Freeman and Company; 2015. p. 449–93.
35. Houten SM, Herrema H, Te BH, Denis S, Ruiter JPN, van Dijk TH, et al. Impaired amino acid metabolism contributes to fasting-induced hypoglycemia in fatty acid oxidation defects. Hum Mol Genet. 2013;22(25):5249–61.
36. Indiveri C, Iacobazzi V, Tonazzi A, Giangregorio N, Infantino V, Convertini P, et al. The mitochondrial carnitine/acylcarnitine carrier: function, structure and physiopathology. Mol Aspects Med. 2011;32(4–6):223–33.
37. Xia C, Fu Z, Battaile KP, Kim JJP. Crystal structure of human mitochondrial trifunctional protein, a fatty acid β-oxidation metabolon. Proc Natl Acad Sci U S A. 2019;116(13):6069–74.
38. Brecher P. The interaction of long-chain acyl CoA with membranes. Mol Cell Biochem. 1983;57(1):3–15.
39. Wang Y, Palmfeldt J, Gregersen N, Makhov AM, Conway JF, Wang M, et al. Mitochondrial fatty acid oxidation and the electron transport chain comprise a multifunctional mitochondrial protein complex. J Biol Chem. 2019;294(33):12380–91.
40. Kerner J, Bieber L. Isolation of a malonyl-CoA-sensitive CPT/. Beta.-oxidation enzyme complex from heart mitochondria. Biochemistry. 1990;29(18):4326–34.
41. Console L, Giangregorio N, Indiveri C, Tonazzi A. Carnitine/acyl-carnitine translocase and carnitine palmitoyltransferase 2 form a complex in the inner mitochondrial membrane. Mol Cell Biochem. 2014;394(1–2):307–14.
42. Paradies G, Paradies V, De Benedictis V, Ruggiero FM, Petrosillo G. Functional role of cardiolipin in mitochondrial bioenergetics. Biochim Biophys Acta - Bioenerg. 2014;1837(4):408–17.
43. Eaton S, Turnbull DM, Bartlett K. Redox control of β-oxidation in rat liver mitochondria. Eur J Biochem. 1994;220(3):671–81.
44. Jin SJ, Hoppel CL, Tserng KY. Incomplete fatty acid oxidation. The production and epimerization of 3-hydroxy fatty acids. J Biol Chem. 1992;267(1):119–25.
45. Nada MA, Rhead WJ, Sprecher H, Schulz H, Roe CR. Evidence for intermediate channeling in mitochondrial β-oxidation. J Biol Chem. 1995;270(2):530–5.
46. Wang Y, Mohsen AW, Mihalik SJ, Goetzman ES, Vockley J. Evidence for physical association of mitochondrial fatty acid oxidation and oxidative phosphorylation complexes. J Biol Chem. 2010;285(39):29834–41.
47. Segel IH. Enzyme kinetics: behavior and analysis of rapid equilibrium and steady-state enzyme systems. 115th ed. New York: Wiley; 1975.
48. Kispal G, Sumegi B, Alkonyi I. Isolation and characterization of 3-hydroxyacyl coenzyme A dehydrogenase-binding protein from pig heart inner mitochondrial membrane. J Biol Chem. 1986;261(30):14209–13.

Odendaal *et al. BMC Biology*   (2023) 21:184

Page 19 of 22

49. Liang X, Le W, Zhang D, Schulz H. Impact of the intramitochondrial enzyme organization on fatty acid oxidation. Biochem Soc Trans. 2001;29(2):279–82.

50. Eaton S, Bursby T, Middleton B, Pourfarzam M, Mills K, Johnson AW, et al. The mitochondrial trifunctional protein: centre of a β-oxidation metabolon? Biochem Soc Trans. 2000;28(2):177–82.

51. Stanley KK, Tubbs PK. The role of intermediates in mitochondrial fatty acid oxidation. Biochem J. 1975;150(1):77–88.

52. Neess D, Bek S, Engelsby H, Gallego SF, Færgeman NJ. Long-chain acyl-CoA esters in metabolism and signaling: role of acyl-CoA binding proteins. Prog Lipid Res. 2015;59:1–25.

53. Rasmussen JT, Færgeman NJ, Kristiansen K, Knudsen J. Acyl-CoA-binding protein (ACBP) can mediate intermembrane acyl-CoA transport and donate acyl-CoA for β-oxidation and glycerolipid synthesis. Biochem J. 1994;299(1):165–70.

54. Kim S, Chen J, Cheng T, Gindulyte A, He J, He S, et al. PubChem in 2021: new data content and improved web interfaces. Nucleic Acids Res. 2021;49(D1):D1388–95.

55. Tetko IV, Bruneau P. Application of ALOGPS to predict 1-octanol/water distribution coefficients, logP, and logD, of AstraZeneca in-house database. J Pharm Sci. 2004;93(12):3103–10.

56. Spiekerkoetter U, Sun B, Zytkovicz T, Wanders R, Strauss AW, Wendel U. MS/MS-based newborn and family screening detects asymptomatic patients with very-long-chain acyl-CoA dehydrogenase deficiency. J Pediatr. 2003;143(3):335–42.

57. Carpenter K, Pollitt RJ, Middleton B. Human liver long-chain 3-hydroxyacyl-coenzyme A dehydrogenase is a multifunctional membrane-bound beta-oxidation enzyme of mitochondria. Biochem Biophys Res Commun. 1992;183(3):443–8.

58. Fraser F, Zammit VA. Enrichment of carnitine palmitoyltransferases I and II in the contact sites of rat liver mitochondria. Biochem J. 1998;329(2):225–9.

59. Schaefer J, Jackson S, Turnbull M, Dick DJ. Trifunctional enzyme deficiency: adult presentation of a usually fatal β-oxidation defect. Ann Neurol Off J Am Neurol Assoc Child Neurol Soc. 1996;40(4):597–602.

60. Brdiczka D. Contact sites between mitochondrial envelope membranes. Structure and function in energy- and protein-transfer. BBA - Rev Biomembr. 1991;1071(3):291–312.

61. Klug GA, Krause J, Östlund A-K, Knoll G, Brdiczka D. Alterations in liver mitochondrial function as a result of fasting and exhaustive exercise. Biochim Biophys Acta - Bioenerg. 1984;764(3):272–82.

62. Wojtczak L, Adams V, Brdiczka D. Effect of oleate on the apparent Km of monoamine oxidase and the amount of membrane-bound hexokinase in isolated rat hepatocytes: Further evidence for the controlling role of the surface charge in hexokinase binding. Mol Cell Biochem. 1988;79(1):25–30.

63. Monné M, Palmieri F. Antiporters of the mitochondrial carrier family. Curr Top Membr. 2014;73:289–320.

64. Palmieri F, Pierri CL. Structure and function of mitochondrial carriers–role of the transmembrane helix P and G residues in the gating and transport mechanism. FEBS Lett. 2010;584(9):1931–9.

65. Cleland WW. An analysis of Haldane relationships. In: Methods in Enzymology. 1982. p. 366–9.

66. Flamholz A, Noor E, Bar-Even A, Milo R. EQuilibrator - The biochemical thermodynamics calculator. Nucleic Acids Res. 2012;40(D1):770–5.

67. Noor E, Bar-Even A, Flamholz A, Lubling Y, Davidi D, Milo R. An integrated open framework for thermodynamics of reactions that combines accuracy and coverage. Bioinformatics. 2012;28(15):2037–44.

68. Kohn MC, Garfinkel D. Computer simulation of metabolism in palmitate-perfused rat heart. I. Palmitate oxidation. Ann Biomed Eng. 1983;11(5):361–84.

69. Modre-Osprian R, Osprian I, Tilg B, Schreier G, Weinberger KM, Graber A. Dynamic simulations on the mitochondrial fatty acid Beta-oxidation network. BMC Syst Biol. 2009;3:1–15.

70. Haraldsdóttir HS, Thiele I, Fleming RMT. Quantitative assignment of reaction directionality in a multicompartment human metabolic reconstruction. Biophys J. 2012;102(8):1703–11.

71. Gustafson WG, Feinberg BA, McFarland JT. Energetics of β-Oxidation. Reduction potentials of general fatty acyl-CoA dehydrogenase, electron transfer flavoprotein, and fatty acyl-CoA substrates. J Biol Chem. 1986;261(17):7733–41.

72. M. Jacobus H. van 't Hoff. Études de dynamique chimique. Recueil des Travaux Chimiques des Pays-Bas. 1884;3(10):333–6.

73. Mendes P, Kell DB, Westerhoff HV. Channelling can decrease pool size. Eur J Biochem. 1992;204(1):257–66.

74. Nic a′ Bháird N, Kumaravel G, Gandour RD, Krueger MJ, Ramsay RR. Comparison of the active sites of the purified carnitine acyltransferases from peroxisomes and mitochondria by using a reaction-intermediate analogue. Biochem J. 1993;294(3):645–51.

75. Ramsay RR, Gandour RD, Van Der Leij FR. Molecular enzymology of carnitine transfer and transport. Biochim Biophys Acta - Protein Struct Mol Enzymol. 2001;1546(1):21–43.

76. McGarry JD, Brown NF. The mitochondrial carnitine palmitoyltransferase system. From concept to molecular analysis. Eur J Biochem. 1997;244(1):1–14.

77. Rohwer JM, Hanekom AJ, Crous C, Snoep JL, Hofmeyr JH. Evaluation of a simplified generic bi-substrate rate equation for computational systems biology. IEE Proceedings-Systems Biol. 2006;153(5):338–41.

78. Wiśniewski JR, Vildhede A, Norén A, Artursson P. In-depth quantitative analysis and comparison of the human hepatocyte and hepatoma cell line HepG2 proteomes. J Proteomics. 2016;136:234–47.

79. Schmidt T, Samaras P, Frejno M, Gessulat S, Barnert M, Kienegger H, et al. ProteomicsDB. Nucleic Acids Res. 2018;46(D1):D1271–81.

80. Fraser F, Padovese R, Zammit VA. Distinct kinetics of carnitine palmitoyltransferase I in contact sites and outer membranes of rat liver mitochondria. J Biol Chem. 2001;276(23):20182–5.

81. van Vlies N, Ruiter JP, Doolaard M, Wanders RJ, Vaz FM. An improved enzyme assay for carnitine palmitoyl transferase I in fibroblasts using tandem mass spectrometry. Mol Gene. 2007;90(1):24–9.

82. Schaefer J, Jackson S, Taroni F, Swift P, Turnbull DM. Characterisation of carnitine palmitoyltransferases in patients with a carnitine palmitoyltransferase deficiency: Implications for diagnosis and therapy. J Neurol Neurosurg Psychiatry. 1997;62(2):169–76.

83. Indiveri C, Tonazzi A, Palmieri F. Identification and purification of the carnitine carrier from rat liver mitochondria. Biochim Biophys Acta - Bioenerg. 1990;1020(1):81–6.

84. Murthy MS, Pande SV. Some differences in the properties of carnitine palmitoyltransferase activities of the mitochondrial outer and inner membranes. Biochem J. 1987;248(3):727–33.

85. Taroni F, Verderio E, Fiorucci S, Cavadini P, Finocchiaro G, Uziel G, et al. Molecular characterization of inherited carnitine palmitoyltransferase II deficiency. Proc Natl Acad Sci U S A. 1992;89(18):8429–33.

86. Miyazawa S, Ozasa H, Furuta S, Osumi T, Hashimoto T. Purification and properties of carnitine acetyltransferase from rat liver. J Biochem. 1983;93(2):439–51.

87. Adeva-Andany MM, Carneiro-Freire N, Seco-Filgueira M, Fernández-Fernández C, Mouriño-Bayolo D. Mitochondrial β-oxidation of saturated fatty acids in humans. Mitochondrion. 2017;2019(46):73–90.

88. Ramsay RR, Naismith JH. A snapshot of carnitine acetyltransferase. Trends Biochem Sci. 2003;28(7):343–6.

89. Chase JF. The substrate specificity of carnitine acetyltransferase. Biochem J. 1967;104(2):510–8.

90. Mittal B, Kurup CKR. Purification of clofibrate-induced carnitine acetyltransferase from rat liver mitochondria. Biochim Biophys Acta - Lipids Lipid Metab. 1980;619(1):90–7.

91. Altamimi TR, Thomas PD, Darwesh AM, Fillmore N, Mahmoud MU, Zhang L, et al. Cytosolic carnitine acetyltransferase as a source of cytosolic acetyl-CoA: a possible mechanism for regulation of cardiac energy metabolism. Biochem J. 2018;475(5):959–76.

92. Finocchiaro G, Ito M, Tanaka K. Purification and properties of short chain acyl-CoA, medium chain acyl-CoA, and isovaleryl-CoA dehydrogenases from human liver. J Biol Chem. 1987;262(17):7982–9.

93. Goetzman ES, Wang Y, He M, Mohsen A-W, Ninness BK, Vockley J. Expression and characterization of mutations in human very-long-chain acyl-CoA dehydrogenase using a prokaryotic system. Mol Genet Metab. 2007;91(2):138–47.

94. Peterson KL, Sergienko EE, Wu Y, Kumar NR, Strauss AW, Oleson AE, et al. Recombinant human liver medium-chain acyl-CoA dehydrogenase: purification, characterization, and the mechanism of interactions with functionally diverse C8-CoA molecules. Biochemistry. 1995;34(45):14942–53.

95. Izai K, Uchida Y, Orii T, Yamamoto S, Hashimoto T. Novel fatty acid β-oxidation enzymes in rat liver mitochondria: I. Purification and properties of very-long-chain acyl-coenzyme A dehydrogenase. J Biol Chem. 1992;267(2):1027–33.

96. Nandy A, Kieweg V, Kräutle FG, Vock P, Küchler B, Bross P, et al. Medium-long-chain chimeric human acyl-CoA dehydrogenase: medium-chain enzyme with the active center base arrangement of long-chain acyl-CoA dehydrogenase. Biochemistry. 1996;35(38):12402–11.

97. Aoyama T, Souri M, Ushikubo S, Kamijo T, Yamaguchi S, Kelley RI, et al. Purification of human very-long-chain acyl-coenzyme A dehydrogenase and characterization of its deficiency in seven patients. J Clin Invest. 1995;95(6):2465–73.

98. Chegary M, te Brinke H, Ruiter JPN, Wijburg FA, Stoll MSK, Minkler PE, et al. Mitochondrial long chain fatty acid β-oxidation in man and mouse. Biochim Biophys Acta - Mol Cell Biol Lipids. 2009;1791(8):806–15.

99. Goetzman ES, Nguyen TV, Vockley. Functional analysis of acyl-CoA dehydrogenase catalytic residue mutants using surface plasmon resonance and circular dichroism. Mol Genet Metab. 2006;87(3):233–42.

100. Nguyen TV, Riggs C, Babovic-Vuksanovic D, Kim YS, Carpenter JF, Burghardt TP, et al. Purification and characterization of two polymorphic variants of short chain acyl-CoA dehydrogenase reveal reduction of catalytic activity and stability of the Gly185Ser enzyme. Biochemistry. 2002;41(37):11126–33.

101. Ikeda Y, Okamura-Ikeda K, Tanaka K. Purification and characterization of short-chain, medium-chain, and long-chain acyl-CoA dehydrogenases from rat liver mitochondria. Isolation of the holo-and apoenzymes and conversion of the apoenzyme to the holoenzyme. J Biol Chem. 1985;260(2):1311–25.

102. Shaw L, Engel PC. The purification and properties of ox liver short-chain acyl-CoA dehydrogenase. Biochem J. 1984;218(2):511–20.

103. Dommes V, Kunau WH. Purification and properties of acyl coenzyme A dehydrogenases from bovine liver. Formation of 2-trans,4-cis-decadienoyl coenzyme A. J Biol Chem. 1984;259(3):1789–97.

104. Kobayashi A, Jiang LL, Hashimoto T. Two mitochondrial 3-hydroxyacyl-CoA dehydrogenases in bovine liver. J Biochem. 1996;119(4):775–82.

105. Fould B, Garlatti V, Neumann E, Fenel D, Gaboriaud C, Arlaud GJ. Structural and functional characterization of the recombinant human mitochondrial trifunctional protein. Biochemistry. 2010;49(39):8608–17.

106. Kiema TR, Harijan RK, Strozyk M, Fukao T, Alexson SEH, Wierenga RK. The crystal structure of human mitochondrial 3-ketoacyl-CoA thiolase (T1): Insight into the reaction mechanism of its thiolase and thioesterase activities. Acta Crystallogr Sect D Biol Crystallogr. 2014;70(12):3212–25.

107. Henson CP, Cleland WW. Kinetic studies of glutamic oxaloacetic transaminase isozymes. Biochemistry. 1964;3(3):338–45.

108. Miyazawa S, Furuta S, Osumi T, Hashimoto T, Up N. Properties of peroxisomal 3-ketoacyl-CoA thiolase from rat liver. J Biochem. 1981;90(2):511–9.

109. Wolters JC, Ciapaite J, Van Eunen K, Niezen-Koning KE, Matton A, Porte RJ, et al. Translational targeted proteomics profiling of mitochondrial energy metabolic pathways in mouse and human samples. J Proteome Res. 2016;15(9):3204–13.

110. Uchida Y, Izai K, Orii T, Hashimoto T. Novel fatty acid beta-oxidation enzymes in rat liver mitochondria. II. Purification and properties of enoyl-coenzyme A (CoA) hydratase/3-hydroxyacyl-CoA dehydrogenase/3-ketoacyl-CoA thiolase trifunctional protein. J Biol Chem. 1992;267(2):1034–41.

111. Jiang LL, Kobayashi A, Matsuura H, Fukushima H, Hashimoto T. Purification and properties of human D-3-hydroxyacyl-CoA dehydratase: medium-chain enoyl-CoA hydratase is D-3-hydroxyacyl-CoA dehydratase. J Biochem. 1996;120(3):624–32.

112. Liang K, Li N, Wang X, Dai J, Liu P, Wang C, et al. Cryo-EM structure of human mitochondrial trifunctional protein. Proc Natl Acad Sci U S A. 2018;115(27):7039–44.

113. Oey NA, Den Boer MEJ, Wijburg FA, Vekemans M, Augé J, Steiner C, et al. Long-chain fatty acid oxidation during early human development. Pediatr Res. 2005;57(6):755–9.

114. Kamijo T, Wanders RJA, Saudubray JM, Aoyama T, Komiyama A, Hashimoto T. Mitochondrial trifunctional protein deficiency. Catalytic heterogeneity of the mutant enzyme in two patients. J Clin Invest. 1994;93(4):1740–7.

115. Middleton B. The mitochondrial long-chain trifunctional enzyme: 2-enoyl-CoA hydratase, 3-hydroxyacyl-CoA dehydrogenase and 3-oxoacyl-CoA thiolase. Biochem Soc Trans. 1994;22(2):427–31.

116. Fong JC, Schulz H. Purification and properties of pig heart crotonase and the presence of short chain and long chain enoyl coenzyme A hydratases in pig and guinea pig tissues. J Biol Chem. 1977;252(2):542–7.

117. He XY, Yang SY, Schulz H. Inhibition of enoyl-CoA hydratase by long-chain l-3-hydroxyacyl-CoA and its possible effect on fatty acid oxidation. Arch Biochem Biophys. 1992;298(2):527–31.

118. Ferdinandusse S, Friederich MW, Burlina A, Ruiter JPN, Coughlin CR, Dishop MK, et al. Clinical and biochemical characterization of four patients with mutations in ECHS1. Orphanet J Rare Dis. 2015;10(1):1–15.

119. Jackson S, Middleton B, Turnbull DM. Characterization of a novel enzyme of human fatty acid β-oxidation: a matrix-associated, mitochondrial 2-enoyl-CoA hydratase. Biochem Biophys Res Commun. 1995;214(1):247–53.

120. Bloisi W, Colombo I, Garavaglia B, Giardini R, Finocchiaro G, Didonato S. Purification and properties of carnitine acetyltransferase from human liver. Eur J Biochem. 1990;189(3):539–46.

121. Miyazawa S, Furuta S, Hashimoto T. Induction of a novel long-chain acyl-CoA hydrolase in rat liver by administration of peroxisome proliferators. Eur J Biochem. 1981;117(2):425–30.

122. Cao J, Xu H, Zhao H, Gong W, Dunaway-Mariano D. The mechanisms of human hotdog-fold thioesterase 2 (hTHEM2) substrate recognition and catalysis illuminated by a structure and function based analysis. Biochemistry. 2009;48(6):1293–304.

123. Yamada J, Kurata A, Hirata M, Taniguchi T, Takama H, Furihata T, et al. Purification, molecular cloning, and genomic organization of human brain long-chain acyl-CoA hydrolase. J Biochem. 1999;126(6):1013–9.

124. Bennett MJ, Spotswood SD, Ross KF, Comfort S, Koonce R, Boriack RL, et al. Fatal hepatic short-chain 1-3-hydroxyacyl-coenzyme dehydrogenase deficiency: Clinical, biochemical, and pathological studies on three subjects with this recently identified disorder of mitochondrial β-oxidation. Pediatr Dev Pathol. 1999;2(4):337–45.

125. Barycki JJ, O'Brien LK, Bratt JM, Zhang R, Sanishvili R, Strauss AW, et al. Biochemical characterization and crystal structure determination of human heart short chain L-3-hydroxyacyl-CoA dehydrogenase provide insights into catalytic mechanism. Biochemistry. 1999;38(18):5786–98.

126. Treacy EP, Lambert DM, Barnes R, Boriack RL, Vockley J, O'Brien LK, et al. Short-chain hydroxyacyl-coenzyme A dehydrogenase deficiency presenting as unexpected infant death: a family study. J Pediatr. 2000;137(2):257–9.

127. Svensson LT, Alexson SEH, Hiltunen JK. Very long chain and long chain acyl-CoA thioesterases in rat liver mitochondria: identification, purification, characterization, and induction by peroxisome proliferators. J Biol Chem. 1995;270(20):12177–83.

128. Moffat C, Bhatia L, Nguyen T, Lynch P, Wang M, Wang D, et al. Acyl-CoA thioesterase-2 facilitates mitochondrial fatty acid oxidation in the liver. J Lipid Res. 2014;55(12):2458–70.

129. Halestrap AP. The regulation of the matrix volume of mammalian mitochondria in vivo and in vitro and its role in the control of mitochondrial metabolism. BBA - Bioenerg. 1989;973(3):355–82.

130. Leonardi R, Rock CO, Jackowski S, Zhang YM. Activation of human mitochondrial pantothenate kinase 2 by palmitoylcarnitine. Proc Natl Acad Sci U S A. 2007;104(5):1494–9.

131. Bekeova C, Anderson-Pullinger L, Boye K, Boos F, Sharpadskaya Y, Herrmann JM, Seifert EL. Multiple mitochondrial thioesterases have distinct tissue and substrate specificity and CoA regulation, suggesting unique functional roles. J Biol Chem. 2019;294(50):19034–47.

132. Bachmann C, Krähenbühl S, Colombo JP. Purification and properties of acetyl-CoA:L-glutamate N-acetyltransferase from human liver. Biochem J. 1982;205(1):123–7.

133. Færgeman NJ, Knudsen J. Role of long-chain fatty acyl-CoA esters in the regulation of metabolism and in cell signalling. Biochem J. 1997;323(1):1–12.

134. Stein LR, Imai SI. The dynamic regulation of NAD metabolism in mitochondria. Trends Endocrinol Metab. 2012;23(9):420–8.

135. Yang H, Yang T, Baur JA, Perez E, Matsui T, Carmona JJ, et al. Nutrient-sensitive mitochondrial NAD+ levels dictate cell survival. Cell. 2007;130(6):1095–107.

136. Beckmann JD, Frerman FE. Reaction of electron-transfer flavoprotein with electron-transfer flavoprotein-ubiquinone oxidoreductase. Biochemistry. 1985;24(15):3922–5.

137. Kunz WS, Gellerich FN. Quantification of the content of fluorescent flavoproteins in mitochondria from liver, kidney cortex, skeletal muscle, and brain. Biochem Med Metab Biol. 1993;50(1):103–10.

138. Nelson DL, Cox MM. Lehninger's principles of biochemistry. Revides Ed. 2005. p. 21–45.

139. Fell DA. Metabolic control analysis: a survey of its theoretical and experimental development. Biochem J. 1992;286(2):313–30.

140. Bakker BM, Michels PAM, Opperdoes FR, Westerhoff HV. Glycolysis in bloodstream form Trypanosoma brucei can be understood in terms of the kinetics of the glycolytic enzymes. J Biol Chem. 1997;272(6):3207–15.

141. Teusink B, Passarge J, Reijenga C, Eshalgado E, van der Weijden CC, Schepper M, et al. Can yeast glycolysis be understood in terms of in vitro kinetics of the constitutent enzyme? Testing biochemistry Eur J Biochem. 2000;267(February):5313–29.

142. Finocchiaro G, Colombo I, DiDonato S. Purification, characterization and partial amino acid sequences of carnitine palmitoyl-transferase from human liver. FEBS Lett. 1990;274(1–2):163–6.

143. Penkler G, Du Toit F, Adams W, Rautenbach M, Palm DC, Van Niekerk DD, et al. Construction and validation of a detailed kinetic model of glycolysis in Plasmodium falciparum. FEBS J. 2015;282(8):1481–511.

144. Du Preez FB, Van Niekerk DD, Kooi B, Rohwer JM, Snoep JL. From steady-state to synchronized yeast glycolytic oscillations I: model construction. FEBS J. 2012;2012(279):2810–22.

145. Abegaz F, Martines ACMF, Vieira Lara MA, Morales MR, Reijngoud DJ, Wit EC, et al. Bistability in fatty-acid oxidation resulting from substrate inhibition. PLoS Comput Biol. 2021;17(8):1–24.

146. Pauly DF, McMillin JB. Importance of acyl-CoA availability in interpretation of carnitine palmitoyltransferase I kinetics. J Biol Chem. 1988;263(34):18160–7.

147. Requero MA, González M, Goñi FM, Alonso A, Fidelio G. Differential penetration of fatty acyl-coenzyme A and fatty acylcarnitines into phospholipid monolayers. FEBS Lett. 1995;357(1):75–8.

148. Peitzsch RM, McLaughlin S. Binding of acylated peptides and fatty acids to phospholipid vesicles: pertinence to myristoylated proteins. Biochemistry. 1993;32(39):10436–43.

149. Cohen Simonsen A, Bernchou Jensen U, Færgeman NJ, Knudsen J, Mouritsen OG. Acyl-coenzyme A organizes laterally in membranes and is recognized specifically by acyl-coenzyme A binding protein. FEBS Lett. 2003;552(2–3):253–8.

150. Knudsen J, Neergaard TBF, Gaigg B, Jensen MV, Hansen JK. The Role of Acyl-CoA Binding protein in acyl-CoA metabolism and acyl-CoA-mediated cell signalling. Am Soc Nutrotional Sci. 2000;130(2):294–8.

151. Smith RH, Powell GL. The critical micelle concentration of some physiologically important fatty acyl-coenzyme A's as a function of chain length. Arch Biochem Biophys. 1986;244(1):357–60.

152. Boylan JG, Hamilton JA. Interactions of acyl-coenzyme A with phosphatidylcholine bilayers and serum albumin. Biochemistry. 1992;31(2):557–67.

153. Prip-Buus C, Thuillier L, Abadi N, Prasad C, Dilling L, Klasing J, et al. Molecular and enzymatic characterization of a unique carnitine palmitoyltransferase 1A mutation in the Hutterite community. Mol Genet Metab. 2001;73(1):46–54.

154. Brunk E, Sahoo S, Zielinski DC, Altunkaya A, Dräger A, Mih N, et al. Recon3D enables a three-dimensional view of gene variation in human metabolism. Nat Biotechnol. 2018;36(3):272–81.

155. Rogers AB, Dintzis RZ. Hepatobiliary system. In: Comparative anatomy and histology. 2018. p. 229–39.

156. Sohlenius-Sternbeck AK. Determination of the hepatocellularity number for human, dog, rabbit, rat and mouse livers from protein concentration measurements. Toxicol Vitr. 2006;20(8):1582–6.

157. Thomas LK, Ittmann M, Cooper C. The role of leucine in ketogenesis in starved rats. Biochem J. 1982;204(2):399–403.

158. Furuta S, Miyazawa S, Hashimoto T. Purification and properties of rat liver acyl-CoA dehydrogenases and electron transfer flavoprotein. J Biochem. 1981;90(6):1739–50.

159. PRIDE - PRoteomics IDEntifications Database: Project PXD001874. 2016. Available from:https://www.ebi.ac.uk/pride/archive/projects/PXD001874. [Cited 2023 Jun 7].

160. JWS Online: odendaal2. Available from: https://jjj.bio.vu.nl/models/odendaal2/simulate/. [Cited 2022 Nov 9].

161. JWS Online: odendaal3. Available from: https://jjj.bio.vu.nl/models/odendaal3/simulate/. [Cited 2022 Nov 9].

162. Siess EA, Brocks DG, Wieland OH. Subcellular distribution of key metabolites in isolated liver cells from fasted rats. FEBS Lett. 1976;69(1–1):265–71.

163. Berg JM, Tymoczko JL, Gatto GL, Stryer L. Oxidative Phosphorylation. In: Berg JM, Tymoczko JL, Gatto GJ, Stryer L, editors. Biochemistry. 8th ed. New York: W.H. Freeman and Company; 2015. p. 523–63.

164. Ran FA, Hsu PD, Wright J, Agarwala V, Scott DA, Zhang F. Genome engineering using the CRISPR-Cas9 system. Nat Protoc. 2013;8(11):2281–308.

165. Fink G, Desrochers S, Des Rosiers C, Garneau M, David F, Daloze T, et al. Pseudoketogenesis in the perfused rat heart. J Biol Chem. 1988;263(34):18036–42.

166. Des Rosiers C, Montgomery JA, Garneau M, David F, Mamer O, Daloze P, et al. Pseudoketogenesis in hepatectomized dogs. Am J Physiol - Endocrinol Metab. 1990;258(3):E519–28.

167. Martines ACMF, Gerding A, Stolle S, Vieira-Lara MA, Wolters JC, Jurdzinski A, et al. Transcriptome analysis suggests a compensatory role of the cofactors coenzyme A and NAD+ in medium-chain acyl-CoA dehydrogenase knockout mice. Sci Rep. 2019;9(1):1–11.

168. Spiekerkötter U, Vockley J. Mitochondrial Fatty Acid Oxidation Disorders. In: Blau N, Ferreira CR, Van Karnebeek CDM, Vici CD, Vianey-Saban C, editors. Physician's guide to the diagnosis, treatment, and follow-up of inherited metabolic diseases. 2nd ed. Cham: Springer; 2022. p. 929–57.

169. van Rijt WJ, van der Ende RM, Volker-Touw CML, van Spronsen F, Derks TGJ, Heiner-Fokkema MR. Changes in pediatric plasma acylcarnitines upon fasting for refined interpretation of metabolic stress. Mol Genet Metab. 2019;127(4):327–35.

170. Brunengraber H, Boutry M, Lowenstein JM. Fatty acid, 3-β-hydroxysterol, and ketone synthesis in the perfused rat liver: effects of (–)-hydroxycitrate and oleate. Eur J Biochem. 1978;82(2):373–84.

171. Touw CML, Smit GPA, de Vries M, de Klerk JBC, Bosch AM, Visser G, et al. Risk stratification by residual enzyme activity after newborn screening for medium-chain acyl-CoA dehydrogenase deficiency: data from a cohort study. Orphanet J Rare Dis. 2012;7(1):1–8.

172. Corydon MJ, Vockley J, Rinaldo P, Rhead WJ, Kjeldsen M, Winter V, et al. Role of common gene variations in the molecular pathogenesis of short-chain Acyl-CoA dehydrogenase deficiency. Pediatr Res. 2001;49(1):18–23.

173. Hoffmann L, Haussmann U, Mueller M, Spiekerkoetter U. VLCAD enzyme activity determinations in newborns identified by screening: a valuable tool for risk assessment. J Inherit Metab Dis. 2012;35(2):269–77.

174. Burrage LC, Miller MJ, Wong L-J, Kennedy AD, Reid Sutton V, Sun Q, et al. Elevations of C14: 1 and C14: 2 plasma acylcarnitines in fasted children: a diagnostic dilemma. J Pediatr. 2016;169:208–13.

175. Costa CG, Dorland L, Tavares de Almeida I, Jakobs C, Duran M, Poll-The BT. The effect of fasting, long-chain triglyceride load and carnitine load on plasma long-chain acylcarnitine levels in mitochondrial very long-chain acyl-CoA dehydrogenase deficiency. J Inherit Metab Dis. 1998;21(4):391–9.

176. Derks TGJ, Boer TS, Assen A, Bos T, Ruiter J, Waterham HR, et al. Neonatal screening for medium-chain acyl-CoA dehydrogenase (MCAD) deficiency in The Netherlands: The importance of enzyme analysis to ascertain true MCAD deficiency. J Inherit Metab Dis. 2008;31(1):88–96.

177. Lampret BR, Murko S, Debeljak M, Tansek MZ, Fister P, Battelino T. A case report of short-chain acyl-CoA dehydrogenase deficiency (SCADD). Biochem Medica. 2015;25(2):279–84.

178. Lisyová J, Chandoga J, Jungová P, Repiský M, Knapková M, Machková M, et al. An unusually high frequency of SCAD deficiency caused by two pathogenic variants in the ACADS gene and its relationship to the ethnic structure in Slovakia. BMC Med Genet. 2018;19(1):1–12.

179. Wolfe L, Jethva R, Oglesbee D, Vockley J. Short-Chain Acyl-CoA Dehydrogenase Deficiency. GeneReviews®. 2018. Available from: https://www.ncbi.nlm.nih.gov/books/NBK63582/. [Cited 2022 Nov 1].

180. Leslie ND, Saenz-Ayala S. Very Long-Chain Acyl-Coenzyme A Dehydrogenase Deficiency. GeneReviews®. 2022. Available from: https://www.ncbi.nlm.nih.gov/books/NBK6816/. [Cited 2022 Nov 1].

Odendaal *et al. BMC Biology*   (2023) 21:184

Page 22 of 22

181. Merritt II JL, Chang IJ. Medium-Chain Acyl-Coenzyme A Dehydrogenase Deficiency. GeneReviews®. 2019. Available from: https://www.ncbi.nlm.nih.gov/books/NBK1424/. [Cited 2022 Nov 1].

182. Quant PA, Makins RA. Metabolic control analysis of hepatic β-oxidation: the top-down approach. Biochem Soc Trans. 1994;22(2):441–6.

183. Quant PA, Robin D, Robin P, Girard J, Brand MD. A top-down control analysis in isolated rat liver mitochondria: can the 3-hydroxy-3-methylglutaryl-CoA pathway be rate-controlling for ketogenesis? BBA - Gen Subj. 1993;1156(2):135–43.

184. Horie S, Isobe M, Suga T. Changes in coa pools in hepatic peroxisomes of the rat, under various conditions. J Biochem. 1986;99(5):1345–52.

185. Staack H, Binstock JF, Schulz H. Purification and properties of a pig heart thiolase with broad chain length specificity and comparison of thiolases from pig heart and Escherichia coli. J Biol Chem. 1978;253(6):1827–31.

186. Kiselevsky YV, Ostrovtsova SA, Strumilo SA. Kinetic characterization of the pyruvate and oxoglutarate dehydrogenase complexes from human heart. Acta Biochim Pol. 1990;37(1):136–9.

187. Ono K, Hakozaki M, Nishimaki H, Kochi H. Purification and characterization of human liver branched-chain α-keto acid dehydrogenase complex. Biochem Med Metab Biol. 1987;37(2):133–41.

188. Kirkby B, Roman N, Kobe B, Kellie S, Forwood JK. Functional and structural properties of mammalian acyl-coenzyme A thioesterases. Prog Lipid Res. 2010;49(4):366–77.

189. Wang W, Palmfeldt J, Mohsen AW, Gregersen N, Vockley J. Fasting induces prominent proteomic changes in liver in very long chain Acyl-CoA dehydrogenase deficient mice. Biochem Biophys Reports. 2016;8(September):333–9.

190. FAIRDOM Hub: Mitochondrial fatty acid oxidation in human liver. https://doi.org/10.15490/fairdomhub.1.investigation.587.1. [Cited 2023 Jun 7].

191. Zhao S, Xu W, Jiang W, Yu W, Lin Y, Zhang T, et al. Regulation of cellular metabolism by protein lysine acetylation. Science (80-). 2010;327(5968):1000–4.

192. Margolis A, Giuliano C. Making the switch: from case studies to N-of-1 trials. Epilepsy Behav Rep. 2019;12:100336.

193. Domenzain I, Sánchez B, Anton M, Kerkhoven EJ, Millán-Oropeza A, Henry C, et al. Reconstruction of a catalogue of genome-scale metabolic models with enzymatic constraints using GECKO 2.0. Nat Commun. 2022;13(1):1–13.

194. Gille C, Bölling C, Hoppe A, Bulik S, Hoffmann S, Hübner K, et al. HepatoNet1: a comprehensive metabolic reconstruction of the human hepatocyte for the analysis of liver physiology. Mol Syst Biol. 2010;6(1):441.

195. Swainston N, Baici A, Bakker BM, Cornish-Bowden A, Fitzpatrick PF, Halling P, et al. STRENDA DB: enabling the validation and sharing of enzyme kinetics data. FEBS J. 2018;285(12):2193–204.

196. Wittig U, Kania R, Golebiewski M, Rey M, Shi L, Jong L, et al. SABIO-RK - Database for biochemical reaction kinetics. Nucleic Acids Res. 2012;40(D1):790–6.

197. Berg JM, Tymoczko JL, Gatto GJ, Stryer L. Fatty Acid Metabolism. In: Berg JM, Tymoczko JL, Gatto GJ, Stryer L, editors. Biochemistry. 8th ed. New York: W.H. Freeman and Company; 2015. p. 643–80.

198. Violante S, IJlst L, Te Brinke H, Koster J, De Almeida IT, Wanders RJA, et al. Peroxisomes contribute to the acylcarnitine production when the carnitine shuttle is deficient. Biochim Biophys Acta - Mol Cell Biol Lipids. 2013;1831(9):1467–74.

199. Scriver CR, Waters PJ. Monogenic traits are not simple: lessons from phenylketonuria. Trends Genet. 1999;15(7):267–72.

200. Dipple KM, Mccabe ERB, Mccabe ERB. Phenotypes of Patients with "Simple" Mendelian disorders are complex traits: thresholds, modifiers, and systems dynamics. Am J Hum Genet. 2000;66(6):1729–35.

201. Dipple KM, Phelan JK, McCabe ERB. Consequences of complexity within biological networks: robustness and health, or vulnerability and disease. Mol Genet Metab. 2001;74(1–2):45–50.

202. Lanpher B, Brunetti-Pierri N, Lee B. Inborn errors of metabolism: The flux from Mendelian to complex diseases. Nat Rev Genet. 2006;7(6):449–60.

203. Faria SS, Morris CFM, Silva AR, Fonseca MP, Forget P, Castro MS, et al. A Timely shift from shotgun to targeted proteomics and how it can be groundbreaking for cancer research. Front Oncol. 2017;7:13.

204. Kontostathi G, Makridakis M, Zoidakis J, Vlahou A. Applications of multiple reaction monitoring targeted proteomics assays in human plasma. Expert Rev Mol Diagn. 2019;19(6):499–515.

205. van Bentum M, Selbach M. An introduction to advanced targeted acquisition methods. Mol Cell Proteomics. 2021;20:100165.

206. Takahashi K, Tanabe K, Ohnuki M, Narita M, Ichisaka T, Tomoda K, et al. Induction of pluripotent stem cells from adult human fibroblasts by defined factors. Cell. 2007;131(5):861–72.

207. Guan Y, Xu D, Garfin PM, Ehmer U, Hurwitz M, Enns G, et al. Human hepatic organoids for the analysis of human genetic diseases. JCI Insight. 2017;2(17):e94954.

208. Sampaziotis F, De Brito MC, Madrigal P, Bertero A, Saeb-Parsy K, Soares FAC, et al. Cholangiocytes derived from human induced pluripotent stem cells for disease modeling and drug validation. Nat Biotechnol. 2015;33(8):845–52.

209. Wang S, Wang X, Tan Z, Su Y, Liu J, Chang M, et al. Human ESC-derived expandable hepatic organoids enable therapeutic liver repopulation and pathophysiological modeling of alcoholic liver injury. Cell Res. 2019;29(12):1009–26.

210. Wu F, Wu D, Ren Y, Huang Y, Feng B, Zhao N, et al. Generation of hepatobiliary organoids from human induced pluripotent stem cells. J Hepatol. 2019;70(6):1145–58.

211. Nagarajan SR, Paul-Heng M, Krycer JR, Fazakarley DJ, Sharland AF, Hoy A, Nagarajan SR, Paul-Heng M, Krycer JR, Fazakerley DJ, Sharland AF, et al. Lipid and glucose metabolism in hepatocyte cell lines and primary mouse hepatocytes: a comprehensive resource for in vitro studies of hepatic metabolism. Am J Physiol - Endocrinol Metab. 2019;316(4):578–89.

212. Hu H, Gehart H, Artegiani B, LÖpez-Iglesias C, Dekkers F, Basak O, et al. Long-term expansion of functional mouse and human hepatocytes as 3D organoids. Cell. 2018;175(6):1591–1606.e19.

213. Cassim S, Raymond VA, Lapierre P, Bilodeau M. From in vivo to in vitro: Major metabolic alterations take place in hepatocytes during and following isolation. PLoS One. 2017;12(12):1–14.

214. Derks TGJ. Fasting Tolerance in MCADD-infants (FiTtINg MCADD). ClinicalTrials.gov. 2019. Available from: https://clinicaltrials.gov/ct2/show/NCT03761693. [Cited 2022 Nov 1].

215. Houten SM, Violante S, Ventura FV, Wanders RJA. The biochemistry and physiology of mitochondrial fatty acid β-oxidation and its genetic disorders. Annu Rev Physiol. 2016;78:23–44.

216. Guide Design Resources [Internet]. Available from: https://web.archive.org/web/20220617144225/https://zlab.bio/guide-design-resources. [Cited 21 August 2023].

217. Dalby B, Cates S, HArris A, Ohki EC, Tilkens ML, Price PJ, et al. Advanced transfection with Lipofectamine 2000 reagent: primary neurons, siRNA, and high-throughput applications. Methods. 2004;33(2):95–103.

218. Heberle AM, Navas PR, Langelaar-Makkinje M, Kasack K, Sadik A, Faessler E, et al. The PI3K and MAPK/p38 pathways control stress granule assembly in a hierarchical manner. Life Sci Alliance. 2019;2(2):1–22.

219. van Zutphen T, Ciapaite J, Bloks VW, Ackereley C, Gerding A, Jurdzinski A, et al. Malnutrition-associated liver steatosis and ATP depletion is caused by peroxisomal and mitochondrial dysfunction. J Hepatol. 2016;65(6):1198–208.

220. Peters M, Eicher JJ, Van Niekerk DD, Waltemath D, Snoep JL. The JWS online simulation database. Bioinformatics. 2017;33(10):1589–90.

221. JWS Online: odendaal1. Available from: https://jjj.bio.vu.nl/models/odendaal1/simulate/. [Cited 2022 Nov 9].

Publisher's Note